

Review

Open Access



Recent processing of interaction mechanisms of single metallic atom/clusters in energy electrocatalysis

Yifan Wei^{1,2}, Huicong Xia^{1,2,*}, Wenfu Yan³, Jia-Nan Zhang^{1,2,*}

¹College of Materials Science and Engineering, Zhengzhou University, Zhengzhou 450001, Henan, China.

²Key Laboratory of Advanced Energy Catalytic and Functional Material Preparation of Zhengzhou City, Zhengzhou 450001, Henan, China.

³State Key Laboratory of Inorganic Synthesis and Preparative Chemistry and College of Chemistry, Jilin University, Changchun 130012, Jilin, China.

*Correspondence to: Prof. Jia-Nan Zhang, College of Materials Science and Engineering, Zhengzhou University, 100 Science Avenue, Zhengzhou 450001, Henan, China. E-mail: zjn@zzu.edu.cn; Dr. Huicong Xia, College of Materials Science and Engineering, Zhengzhou University, 100 Science Avenue, Zhengzhou 450001, Henan, China. E-mail: hcxia9209@zzu.edu.cn

How to cite this article: Wei Y, Xia H, Yan W, Zhang JN. Recent processing of interaction mechanisms of single metallic atom/clusters in energy electrocatalysis. *Energy Mater* 2023;3:300033. <https://dx.doi.org/10.20517/energymater.2023.13>

Received: 9 Mar 2023 **First Decision:** 4 Apr 2023 **Revised:** 9 Apr 2023 **Accepted:** 12 Apr 2023 **Published:** 5 Jul 2023

Academic Editor: Yuhui Chen **Copy Editor:** Fangling Lan **Production Editor:** Fangling Lan

Abstract

Understanding the interactions between single metallic atom/clusters (SMACs) has been taken to an unprecedented level, due to the delicate conditions required to produce exotic phenomena in electrode materials, such as thermocatalysis, electrocatalysis, and energy storage devices. Recently, state-of-the-art synthesis methods, such as one-step pyrolysis and multistep pyrolysis, have been developed for SMACs. Herein the interactions between SMACs such as synergetic, charge redistribution effects, and mutual assistance effects, are studied. SMACs have the advantage of maximum utilization of atoms and scattered active sites compared to single metal atoms, and they also have flexible and tunable atom clusters. SMACs have been widely developed and have shown excellent catalytic performance in electrocatalysis. Herein, the self-interaction between SMACs and their catalytic mechanisms are systematically described. The challenges in current synthesis strategies, catalytic mechanisms, and industrial applications of SMACs are analyzed, and a possible synthesis method for SMACs is proposed.

Keywords: Single metallic atom/clusters, interactions, mechanism, synthetic strategy, energy electrocatalysis



© The Author(s) 2023. **Open Access** This article is licensed under a Creative Commons Attribution 4.0 International License (<https://creativecommons.org/licenses/by/4.0/>), which permits unrestricted use, sharing, adaptation, distribution and reproduction in any medium or format, for any purpose, even commercially, as long as you give appropriate credit to the original author(s) and the source, provide a link to the Creative Commons license, and indicate if changes were made.



INTRODUCTION

Driven by the dual-carbon strategy, electrochemical energy is the source of power for promoting and realizing modernization as well as for the steady growth of the economy in China^[1-3]. To mitigate environmental problems and the energy crisis, electrochemical catalytic reactions, such as hydrogen evolution reaction (HER)^[4-6], oxygen evolution reaction (OER)^[7], oxygen reduction reaction (ORR)^[8], carbon dioxide reduction reaction (CO₂RR)^[9-11], nitrogen reduction reaction (NRR)^[12], and nitrate reduction reaction (NITRR)^[13] have attracted great attention. Understanding the catalyst synthesis and reaction mechanism is vital for the development of electrochemistry. Catalytic reaction mechanisms in electrochemical energy engineering have recently attracted research attention^[14]. Inhomogeneous catalysis has contributed to catalyst diversity and the development of several industries that require multiple complex chemical catalytic processes, such as the energy and environmental industries^[15]. Multiphase catalysts also play a key role in environmental pollution problem-solving, green chemistry, and energy storage processes^[16]. Despite tremendous developments in the research of catalysts, many challenges still need to be addressed. Insufficient catalytic activity limits the efficiency of industrial production^[17]. Catalytic selectivity is also an important indicator for reducing molecular separation costs^[18]. Poor catalyst lifetime, i.e., stability, leads to environmental pollution and significantly increases the cost, which can directly hinder its large-scale application^[19-21].

In heterogeneous catalysis, the interaction between gas-phase reactants and solid-phase catalysts occurs at the active sites on the solid surface^[22-24]. Increasing the number of active sites on the catalyst surface is a direct way to improve catalytic efficiency^[25]. Single metallic atom (SMA) site catalysts, characterized by maximum atom utilization and isolated active sites, have recently been extensively researched. It should be noted that the single metallic atom sites discussed in this review do not only refer to the atoms that coordinate with heteroatoms (such as carbon, nitrogen, sulfur, and oxygen), but also include the sites that form mono-atomic alloy catalysts with other metallic elements. The ratio of surface metal atoms to total metal atoms of these catalysts can theoretically be increased to 100%, corresponding to that of fully exposed cluster catalysts^[26-28]. Over the past few decades, various methods have been proposed to modify SMA catalyst structures at the atomic level to achieve high metal site density, suitable *d*-band centers, and optimal binding strength to reactant intermediates^[29]. Although catalysts with fully exposed active sites have excellent catalytic activity, their synthesis and stability cannot be controlled during catalysis. Metal atoms agglomerate due to high-temperature pyrolysis during SMA synthesis^[30]. Thus, the synthesis of SMA requires precise control of the pyrolysis temperature after the metal atoms are agglomerated, which leads to the atomic recovery rate decreasing dramatically. In addition, SMA catalysts are extremely sensitive to the environment and detach from metal sites by acidic electrolytes, which can degrade their catalytic activity. In fact, the pH of the catalytic environment can greatly affect the catalytic activity. ORR, for example, is limited by proton-coupled electron transfer at pH below 10.5. At higher pH values, the reaction occurs in the outer Helmholtz plane (OHP), which is conducive to the production of H₂O₂^[31,32].

Unlike SMA catalysts, interactions in single metallic atom/clusters (SMACs) are crucial for enhancing the catalytic activity of materials^[33,34]. Here, we define the block interacting with the single atomic site as cluster. In the traditional definition of cluster, the size often determines the catalytic performance to a large extent. In order to cover a wide range of interaction mechanisms, clusters mentioned in this paper are not limited to subnanometer or nanometer sizes. Thus, the electronic structure and chemical state of catalytic sites on the catalyst surface can be modified using SMACs^[35]. To ensure low active-site density, metal sub-nano clusters are loaded, which change the electronic states of the active sites and the electronic structure of the surface^[36,37]. However, this interaction mechanism has not been discussed in detail and is referred to as the synergistic effect. This synergistic effect exists between active sites and intermediates, which optimize their

electronic structure and binding behavior, respectively [Scheme 1].

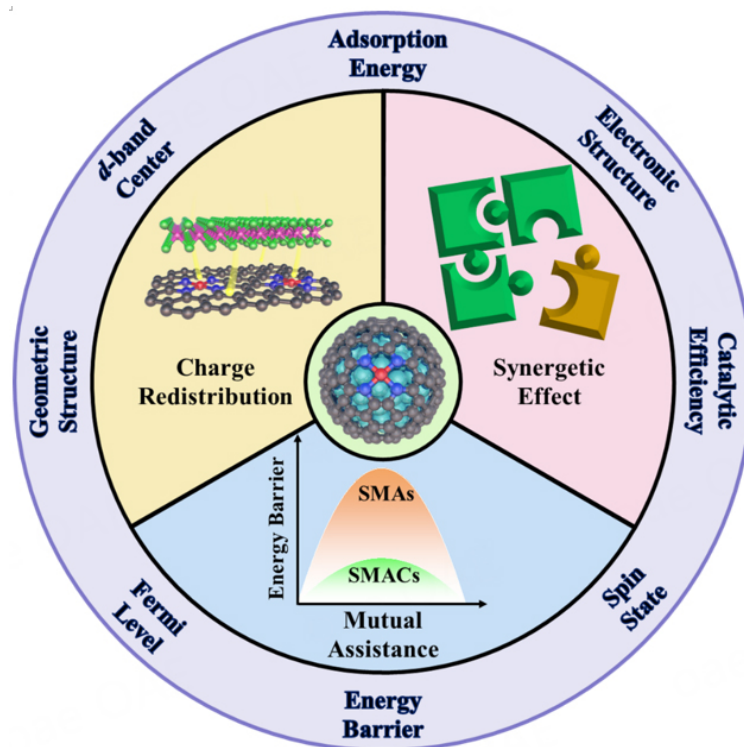
The synthesis, structural modification, performance implications, and specific applications of cluster or SMA catalysts have been reported previously reported^[38,39]. Herein, the advantages and disadvantages, fabrication methods, interactions, and catalytic mechanisms of SMACs are described. We classify the catalytic mechanisms of SMACs into synergistic effects, charge redistribution effects, and mutual assistance. The charge redistribution effect includes charge transfer, strong electronic coupling effect, and spin state adjustment. SMACs interactions are studied to understand their catalytic effects. Finally, the challenges and prospects of SMACs in industrial applications are discussed. The results of this study will pave the way for the research of SMACs as energy electrocatalysts.

SYNTHETIC STRATEGY OF SINGLE METALLIC ATOM/CLUSTERS ELECTROCATALYST

SMACs have unique structural characteristics that enable their interaction with atomically dispersed metals, coordination atoms on the carriers such as N^[40], O^[41], S^[42], and P^[43], and atomic clusters on the carrier, thereby playing a vital role in enhancing catalytic activity and stability. In addition to carbon, SiO₂^[44] and P^[45] can be used as the carrier^[46-51]. In SMA catalysts, single atomic sites are often artificially generated to form clusters during pyrolysis, which affects their catalytic activity. However, the catalytic process can be modified using metal clusters, thereby enhancing the catalytic performance of SMACs.

SMACs are synthesized *via* several methods such as one-step pyrolysis^[52], multi-stage pyrolysis^[53], including atomic layer deposition (ALD)^[54], and pyrolytic-liquid phase loading strategy^[55]. Most of these methods use metal precursors (e.g., metal nitrates^[56], metal chlorides^[57], and metal-organic frameworks (MOFs)^[58]) as starting materials. For instance, Xia *et al.* synthesized the sulfurization of Fe-N-C catalyst containing Fe_xC/Fe species (FeNC-S-Fe_xC/Fe) by a one-step pyrolysis method [Figure 1A]^[59]. Fe_xC/Fe clusters, Fe-C and C-S-C bonds enhanced the FeN_x active sites, making FeNC-S-Fe_xC/Fe a high-performance dual-function catalyst for Zn-air batteries (ZABs). Moreover, Xia *et al.* used the same strategy to modify the ratio of Fe_{sA} sites to clusters by controlling the pyrolysis temperature and used it in sodium-ion batteries (SIBs)^[60]. In addition to Fe, Co, is commonly used as a precursor to synthesize SMACs *via* one-step pyrolysis. Zhao *et al.* synthesized single-atom Co-C₃N₄ nanosheets *via* one-step pyrolysis of a mixture of melamine and cobalt precursors^[61]. The Fe₂O₃/Co-C₃N₄ nanosheets could significantly improve the photoelectrochemical water oxidation activity of Fe₂O₃ photoanodes. However, during pyrolysis, metal agglomeration could not be controlled by heating, causing excessive clustering. Ma *et al.* controlled the size of the metal clusters by further etching after pyrolysis, improving their ability to obtain singlet oxygen (¹O₂), which then promoted the formation of imines and reduced the reaction energy for barrier^[62]. One-step pyrolysis is used for clusters and single-atoms containing the same elements, whereas multistep pyrolysis is used for controlling different elements and morphologies. Guo *et al.* synthesized Co₂P-CoN double-active centers confined in N-doped carbon nanotube [Figure 1C]^[45]. The catalyst can be used as an efficient trifunctional electrocatalyst for HER, ORR, OER, and ZABs. Furthermore, Xue *et al.* also used a one-step pyrolysis method to load Ir clusters onto N\B doped defective carbon, and successfully synthesized Ir@NBD-C with excellent hydrogen evolution performance [Figure 1B]^[63]. The formation of some SMA requires the preparation of specific templates by pyrolysis. Yin *et al.* prepared SBA-15 *via* one-step pyrolysis as a template for the fabrication of NiNC structures and used nickel acetylacetonate as a nickel source for further pyrolysis to obtain a Cu/Ni nitrogen assembly carbon^[64].

Unlike transition metals, noble metals are often loaded onto different carriers *via* deposition. ALD is a widely used synthesis technique used to effectively obtain the SMA sites of noble metals on carrier materials. Liu *et al.* obtained monatomic catalysts using multiple ALD techniques to deposit Ni on the SiO₂



Scheme 1. The interaction mechanisms of single metallic atom/clusters in energy electrocatalysis.

substrate^[44]. The quasi Pd₁Ni single-atom surface alloy forming after multiple deposition cycles. In similar research, Liu *et al.* used Ag as the substrate to deposit palladium diacetylacetonate and trimethylgallium atomic layer under an oxygen environment to obtain Pd SAM catalysts^[44]. Thus, these methods can be used for the successful synthesis of SMACs. SMACs can also be synthesized by liquid deposition of pyrolyzed carriers. Xiao *et al.* prepared SMA *via* one-step pyrolysis and evenly dispersed them in water. To this, H₂PtCl₆·6H₂O was added and Pt/Fe-N-C electrocatalyst was synthesized *via* reactive deposition^[65]. The deposition of noble metals in the liquid phase followed by one-step pyrolysis (or using single atomic site catalysts) is a widely used method for SMACs synthesis. This synthesis method allows controlling the size of noble metal nanoclusters by controlling the number of noble metals added and the liquid phase environment.

In addition to the common SMACs synthesis strategies described above, there are many other approaches. For example, Zhang *et al.* deposited Pt onto MoC using the incipient wetness impregnation method, and then defects in MoC acted as anchor sites to effectively trap Pt atoms^[66]. Qiao *et al.* synthesized Pt₁/FeO_x catalysts *via* CO oxidation using Pt^[67]. The strong electron transfer between Pt and FeO_x makes atomically dispersed Pt a catalytic site for promoting CO oxidation. Similarly, noble metal atoms can effectively bind to defects to form atomically dispersed noble-metal active sites. This synthesis strategy applies to not only metal-based materials, but also nonmetallic substrates. [Scheme 2](#) shows these synthesis methods, among which pyrolysis is widely used. Pyrolysis is the most used method, which has strong universality. However, due to the limitation of metal agglomeration, the heating rate and temperature must be accurately controlled. To this end, multistep pyrolysis or noble metal loading must be used for controlling the catalyst morphology after pyrolysis. ALD can accurately control the atomic layer thickness and the number of exposed SMA sites at low temperatures but at the expense of high synthesis cost, which limits its wide applicability.

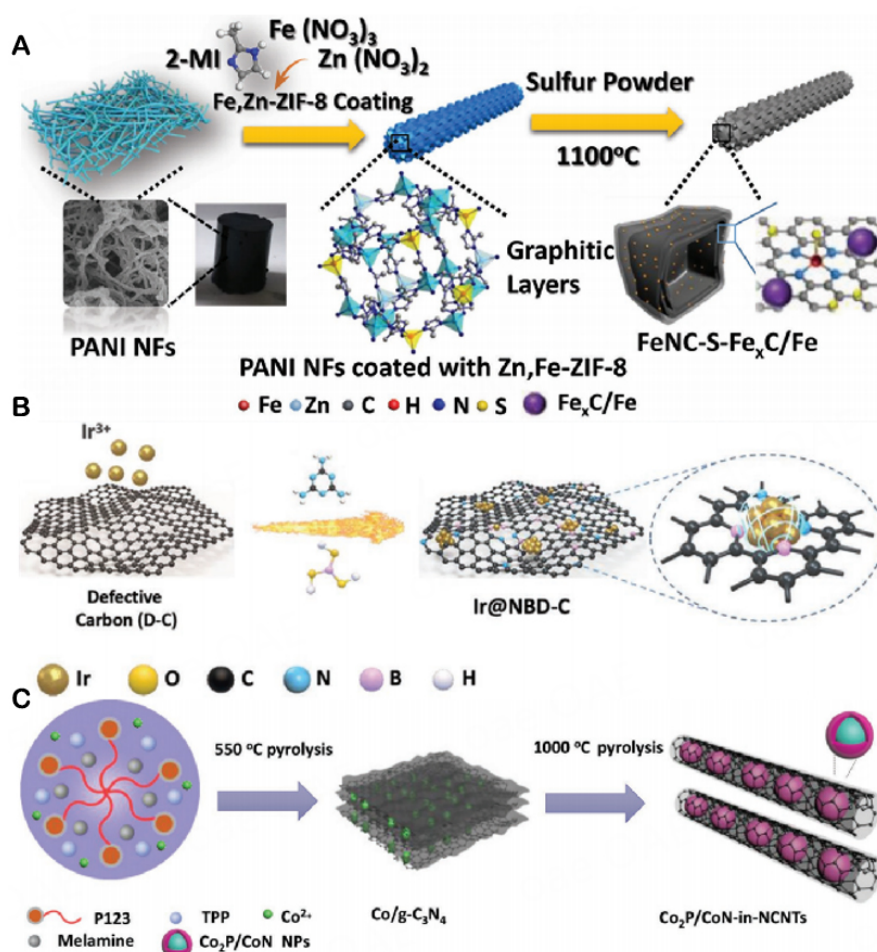
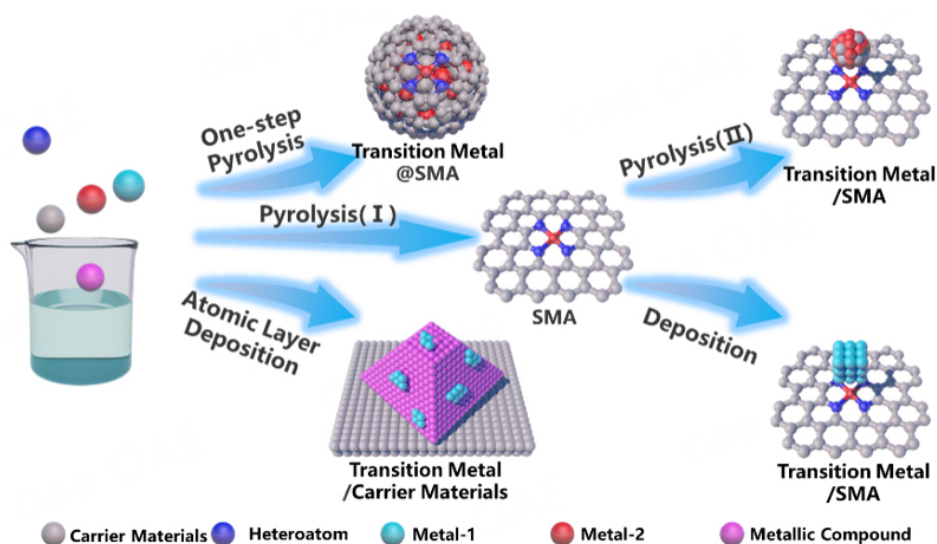


Figure 1. Synthesis scheme. (A) FeNC-S- $\text{Fe}_x\text{C}/\text{Fe}$ catalysts. Reproduced with permission from Ref. [59], © WILEY-VCH Verlag GmbH & Co. KGaA, Weinheim 2018. (B) Ir@NBD-C catalysts. Reproduced with permission from Ref. [63], © WILEY-VCH Verlag GmbH & Co. KGaA, Weinheim 2022. (C) $\text{Co}_2\text{P}/\text{CoN-in-NCNTs}$ catalysts. Reproduced with permission from Ref. [45], © WILEY-VCH Verlag GmbH & Co. KGaA, Weinheim 2018.

INTERACTION MECHANISM OF SINGLE METALLIC ATOM/CLUSTERS ELECTROCATALYSTS

Synergetic effect of single metallic atom/clusters catalysts interactions

The design and fabrication of heterogeneous solid catalysts containing multiple components have attracted research attention^[68-71]. Appropriate combination of different elements significantly improves the catalytic performance, which is considerably higher than that of the individual elements. The application of conventional SAM in electrocatalytic energy reactions is limited by their ability to optimize the Gibbs free energy (Δ_G) for a single reaction, which affects the electrocatalytic energy reaction kinetics. This challenge can be overcome by the synergistic effect of single-metal active sites and cluster sites, which reduces the energy barrier in multiple reaction steps^[72]. In this paper, the synergetic effect is divided into “tandem catalysis” and “concerted catalysis”. Tandem catalysis, as the name suggests, is similar to the series of electrical appliances in a circuit in which the reaction intermediates proceed through the different steps of the catalytic process at different reaction points. Different from tandem catalysis, collaborative catalysis occurs as a result of simultaneous action of multiple components without multiple active sites.



Scheme 2. The synthetic process of single metallic atom/clusters.

Tandem catalysis

Multi-site catalytic are used for tandem catalysis. In multi-catalytic processes, different catalytic sites are only effective for specific catalytic steps. Using this characteristic, different catalysts can be combined to synthesize catalysts to perform different catalytic steps. Liu *et al.* fabricated a series of electrodes based on Rh as a single active site and clusters supported on Cu nanowires (Rh@Cu NWs) *via* the synergistic effect^[73], resulting in high catalytic activity. The hydrogen adsorbed on Rh sites is transferred to vicinal NO intermediate species on Cu sites, promoting hydrogenation reaction and ammonia formation [Figure 2A]. To demonstrate the “division of labor” between Rh and Cu sites during catalysis, the formation of hydrogen radicals during HER was monitored by electron paramagnetic resonance (EPR) using dimethyl-1-pyrroline-N-oxide (DMPO) as the radical trapping reagent. Comparison of the EPRs of electrolytes with and without NO₃⁻ reveals that H-DMPO is formed in the electrolyte without NO₃⁻, and the same trend is observed for HER performance [Figure 2B]. The H-DMPO signal did not change for the electrolyte containing NO₃⁻ and sample Rh nanoparticles (NPs), confirming that Rh NPs are barely active toward nitrate reduction reaction, whereas H⁺ in Rh@Cu-0.6% and Cu NWs are consumed quickly. On the other hand, *in situ* infrared spectroscopy (IR) results show only a weak characteristic peak corresponding to -NH₂ from -0.1 V *vs.* RHE when pure Cu NWs catalyze NITRR [Figure 2C]. An obvious characteristic peak corresponding to -NH₂ is detected from 0.2 V *vs.* RHE when Rh@Cu-0.6% catalyzes NITRR. This corroborates the EPR results, Rh shows a near-optimal ΔG_{H^+} . Thus, the addition of Rh greatly improves H⁺ adsorption on the electrode surface, which can promote the hydrogenation of NO^{*} at the nearby Cu site at a lower application potential. The synergistic effect of Rh and Cu sites was theoretically verified using the density functional theory (DFT) calculation of the stepwise deoxygenation reaction and hydrogenation process, $^*NO_3 \rightarrow ^*NO_2 \rightarrow ^*N$ and $^*NO \rightarrow ^*NOH \rightarrow ^*NH_2OH \rightarrow ^*NH_3$, in the NITRR process [Figure 2D]. The addition of Rh considerably reduces the amount of intermediate *NOH formed, which is the rate-determining step (RDS) of NITRR.

SMACs show great potential as electrocatalysts for fundamental reactions, such as ORR and OER, in proton-exchange membrane fuel cells (PEMFCs). Ding *et al.* reported the synthesis of a bi-functional oxygen electrocatalyst by combining Fe_{SA} and NiCo NPs in carbon nanotubes (CNTs) for fabricating efficient and long-life rechargeable ZABs^[74]. Similar to PEMFCs, ZABs use ORR and OER. The WT contour plot of FePc|CNTs||NiCo/CP is similar to that of FePc, implying that the N coordination of Fe atoms exists

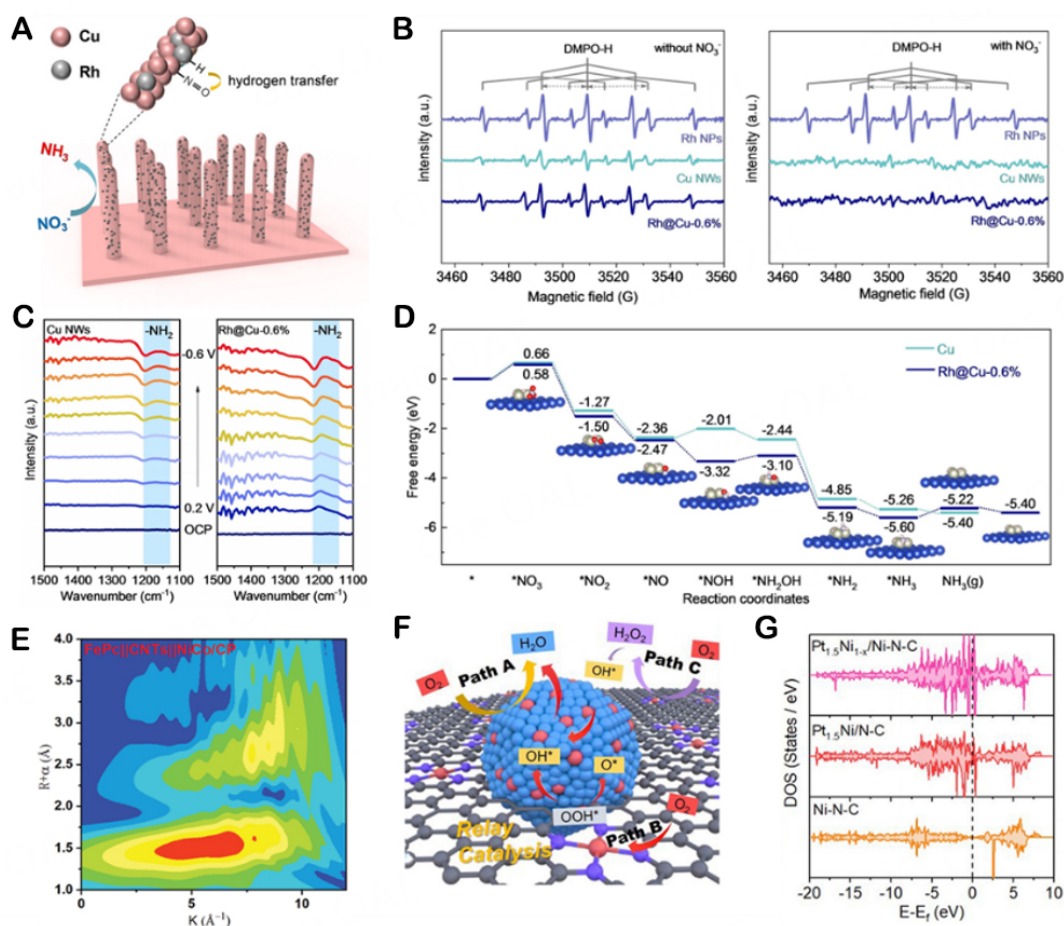


Figure 2. (A) Schematic diagram of the Rh@Cu-0.6% nitrate reduction reaction. (B) Electron paramagnetic resonance (EPR) spectra of the solutions obtained after 3 min of electrocatalysis at -0.1 V vs. RHE by Cu NWs, Rh@Cu-0.6% and Rh NPs loading on carbon cloth in 0.1 M Na_2SO_4 electrolyte with/without 0.1 M KNO_3 under argon. (C) Electrochemical *in situ* infrared spectroscopy (IR) of Rh@Cu-0.6% and Cu NWs with different potentials at 0.1 M Na_2SO_4 electrolyte with 0.1 M KNO_3 . (D) Gibbs free energy diagram of various intermediates generated during electrocatalytic NITRR over the pure Cu NWs and Rh@Cu-0.6%, it is assumed that all Rh in Rh@Cu-0.6% exists in the form of clusters. The structural models represent the adsorption form of various intermediates on Rh@Cu-0.6% during NITRR, Cu blue, Rh light gray, N light blue, O red, and H light pink atoms. Reproduced with permission from Ref. [73], © WILEY-VCH Verlag GmbH & Co. KGaA, Weinheim 2022. (E) Wavelet transform (WT) of FePc|[CNTs]|NiCo/CP. Reproduced with permission from Ref. [74], © WILEY-VCH Verlag GmbH & Co. KGaA, Weinheim 2022. (F) Schematics of $\text{Pt}_{1.5}\text{Ni}_{1-x}/\text{Ni-N-C}$ (blue, red, purple, and gray spheres present Pt, Ni, N, and C atoms, respectively) (G) the total density of states and the corresponding *d*-band centers of $\text{Pt}_{1.5}\text{Ni}_{1-x}/\text{Ni-N-C}$, $\text{Pt}_{1.5}\text{Ni}/\text{Ni-N-C}$, and Ni-N-C . The Fermi level is marked with a black dashed line. The *d*-band center is marked with a purple line. Reproduced with permission from Ref. [75], © The Royal Society of Chemistry 2023.

as a single atom. In addition, the FT k^3 -weighted EXAFS and Fe K-edge XANES spectra of FePc|[CNTs]|NiCo/CP demonstrated that Fe in the sample forms a Fe-N bond instead of a Fe-Fe bond, indicating the existence of Fe atom site [Figure 2E]. Electrochemical performance tests of ZABs revealed ORR and OER as the two central reactions, with the ORR half-wave potential ($E_{1/2@ORR}$) of 0.902 V, which is significantly higher than that of the Pt/C catalyst (0.842 V), and the OER potential ($E_j = 10$) of 1.588 V at a current density of 10 mA cm^{-2} , which is considerably better than that of the Ir/C catalyst (1.608 V). The excellent oxygen electrocatalytic properties are due to the presence of Fe_{SA} and NiCo hydroxide sites, which accelerate the ORR and OER, respectively.

Guo *et al.* reported that the initial Pt_{1.5}Ni NC undergoes a dealloying process driven by ammonia and heat, as the nickel atoms are continuously separated from the substrate to form a stable Pt surface Pt_{1.5}Ni_{1-x} alloy^[75]. Subsequently, these Ni atoms will be captured by adjacent defects on the carbon substrate, resulting in many NiSA sites that are closely distributed around the de-alloyed Pt_{1.5}Ni_{1-x}. The morphologies of PtNi alloys at different stages can be observed *via* morphological characterization in addition to the valence states and coordination environments of Ni and Pt. The white line intensity of the Ni K-edge gradually increased and the absorption threshold position shifted toward Ni³⁺, indicating that Ni was further oxidized. The half-wave potential ($E_{1/2}$) of Pt_{1.5}Ni_{1-x}/Ni-N-C in 0.1 M HClO₄ solution is 0.967 V, which is higher than that of the commercial Pt/C (0.887 V). **Figure 2F** shows the synergistic effect of different sites within the Pt_{1.5}Ni_{1-x}/Ni-N-C, indicating superior ORR performance. The yellow arrow in the figure shows the reaction pathway A, where ORR occurs *via* a four-electron transfer pathway at the Pt site to yield H₂O. A two-electron transfer reaction occurs at the Ni-N-C site to produce hydrogen peroxide (path C). However, for the NiSA sites near the Pt_{1.5}Ni_{1-x}, the resulting OOH^{*} is directly adsorbed by the Pt site, undergoing further reaction to form H₂O. By calculating the density of states of the Pt_{1.5}Ni_{1-x}/Ni-N-C and other comparison samples, it is revealed that there are abundant electron states near the Fermi-level of the samples; this indicates a possible electron interaction between the PtNi clusters and Ni-N-C sites [**Figure 2G**].

Concerted catalysis

Using the Ru-alginate metal-organic supramolecular conversion method, Zhang *et al.* synthesized an electrocatalyst containing both Ru single atoms (SAs) and NPs anchored on defective carbon (Ru_{SA+NP}/DC)^[76]. XAS spectra of Ru_{SA+NP}/DC, metallic Ru, and RuO₂ proved that Ru_{SA+NP}/DC contains Ru-Ru metallic bonds and Ru-C bonds. Differential charge density distributions revealed that the charge is transferred from the Ru atom to the H₂O molecule [**Figure 3A**]. This charge transfer significantly elongates the H-O bond of the adsorbed water to 0.983 Å, implying that Ru NPs have an important positive promoting effect on hydrolytic splitting. H⁺ adsorption energies of different Ru catalysts were calculated. The volcano plot [**Figure 3B**] shows that Ru_{NP}@DC-2 and Ru (001) exhibit more negative ΔE_{H^+} values. Such strong adsorption led to a relatively high overpotential of HER (η_{HER}). The ΔE_{H^+} of Ru_{SA}@DC-1 is closer to the center of the volcano plot. **Figure 3C** shows that the energy barrier for the water splitting of Ru_{SA}@DC-1 and Ru_{SA}@DC-2 are as high as 1.09 and 1.12 eV, respectively. This suggests that Ru SA is insufficient for dissociating the H-OH bond, whereas Ru_{NP}@DC-1 can efficiently dissociate water and facilitate HER. Similarly, conjugated structures of different atoms can be adjusted to enhance the interaction between single atoms and clusters. Su *et al.* successfully constructed a composite nanoreactor containing SMAs, carbon substrate, and Ru NPs by doping oxygen-containing graphene with Fe, Co, Ni, and other SMAs and using it as a carrier to support Ru NPs [**Figure 3D**]^[77]. First-principles calculation shows that SMA (Fe, Co, and Ni) modification can lead to the redistribution of surface charge of oxygen-containing graphene, resulting in an electron-deficient state of carbon atoms around the single atom; this will significantly enhance HER properties at the site of Ru NPs.

Yang *et al.* designed a novel catalyst containing Ir NPs and atomic Ir sites (Ir_{NP}@Ir_{SA}-N-C), which could effectively address the CO poisoning problem of the catalyst^[78]. The EXAFS signals of Ir_{NP}@Ir_{SA}-N-C show the existence of Ir_{NP} and Ir_{SA} [**Figure 3E** and **F**]. The atomic Ir site, a good CO oxidation site, efficiently removes CO molecules adsorbed on Ir_{NP} in a short time. Thus, Ir_{NP} retains part of the active site, which is conducive to promoting H₂ oxidation. The interaction between Ir_{NP} and Ir_{SA} centers enhances the H₂ oxidation activity of the catalyst and the electrooxidation activity of CO in PEMFCs [**Figure 3G**].

Charge redistribution effect of single metallic atom/clusters electrocatalysts

The redistribution of charge on the catalyst surface is the design idea for most catalysts, particularly SMACs. Charge redistribution can change the charge density of active sites and thus change the charge distribution

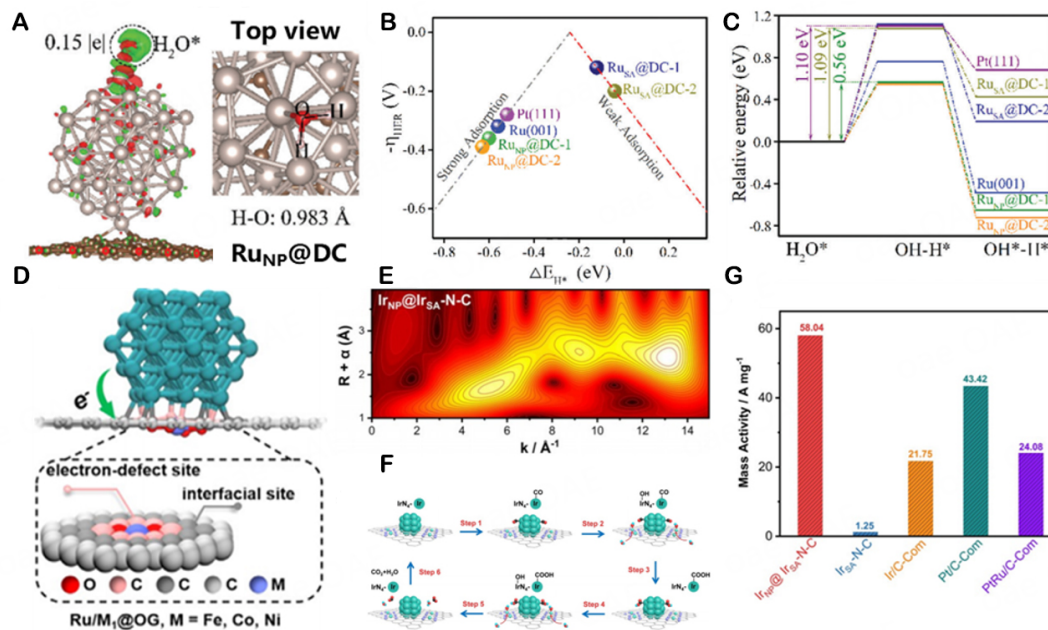


Figure 3. (A) Differential charge density distributions of active Ru atom for RuNP@DC-1 and adsorbed H₂O. (B) Volcano plot of theoretical η_{HER} vs. ΔE_{H^*} . (C) Kinetic barrier of H₂O dissociation for different models. Reproduced with permission from Ref. [76], © WILEY-VCH Verlag GmbH & Co. KGaA, Weinheim 2021. (D) Atomic structures of Ru₅₅ supported on O-doped graphene with dispersed metal atoms obtained by DFT calculations. (E) Wavelet transforms for the k^2 -weighted EXAFS signals of Ir_{NP}@Ir_{SA}-N-C. (F) Schematic illustration of the synergistic effect mechanism between IrN₄ sites and Ir NPs. (G) The metal mass activities of different catalysts at 0.6 V in H₂-O₂ PEMFC.

around the Fermi level^[79-82]. The d -band center of the active core metal can also be changed to optimize the reaction path and activation energy. Moreover, the reaction process can be optimized by changing the adsorption-desorption strength of the reaction intermediates through strong electron coupling between different active sites. The spin state of the active site can be modified by charge redistribution to further accelerate energy electrocatalysis^[83].

Charge transfer

Xia *et al.* showed the fabrication of Fe-N-C graphitic layer-encapsulating Fe₃C species within carbon nanosheets (Fe-N-C/Fe₃C@HCNs) *via* one-step pyrolysis^[60]. The SMA active sites can be clearly observed by morphological characterization. In addition, the NEXAFS shows that the coordination forms of Fe in the catalyst system are Fe-N, Fe-Fe, and Fe-C, respectively, which proves the existence of the Fe-N-C site and Fe₃C. Figure 4A and B show the density of state (DOS) illustrations of Fe-N-C/Fe₃C and Fe-N-C. Compared with Fe-N-C, the electron states near the Fermi level of Fe-N-C/Fe₃C increase significantly under pre- and post-treatment conditions. This indicates that the electron mobility in Fe-N-C/Fe₃C is improved, which significantly reduces the charge transfer resistance. Figure 4C shows the schematic after long-life cycles, which can be proved to be structurally complete without collapse through the image of an electron microscope.

For SMACs, the size of clusters will considerably affect the degree of electron transfer and the catalytic performance. Huang *et al.* synthesized Fe-based metal-organic frameworks (Fe-MOFs) with nanocube structures using the co-precipitating method^[84]. The Fe-MOFs were then coated by polydopamine *via* the self-polymerization of the dopamine monomer in alkaline conditions. Then, two-step pyrolysis was performed under ammonia and Ar gas flows successively to increase the N content and enhance

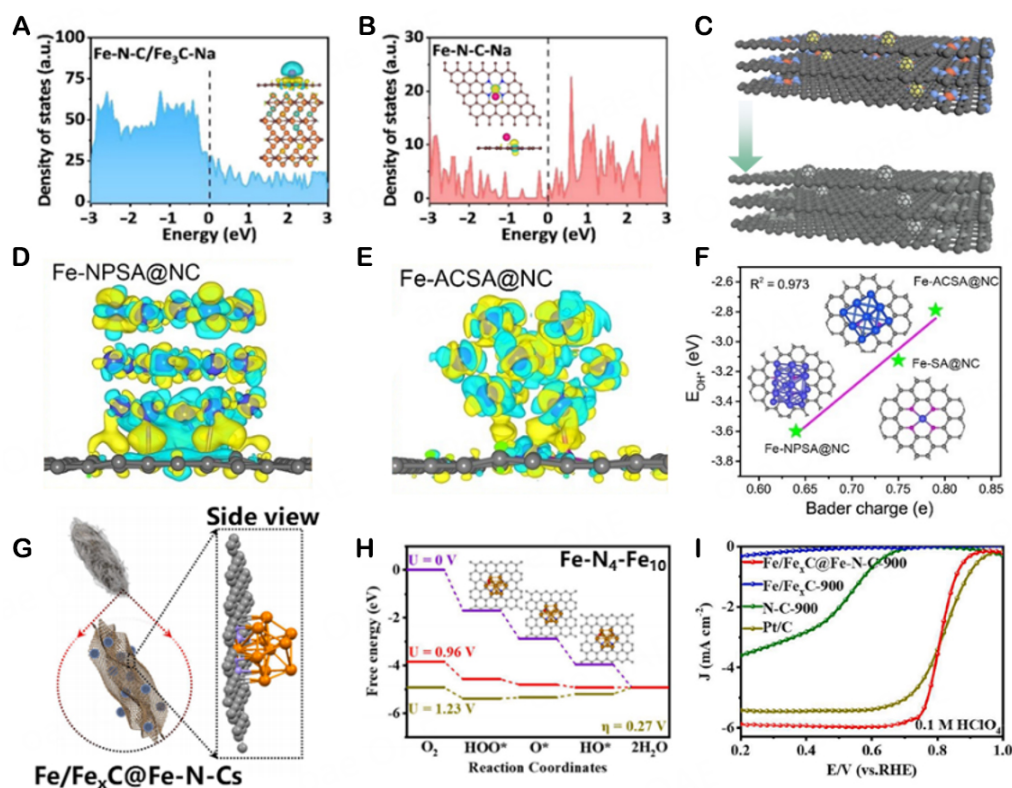


Figure 4. (A and B) DOS illustrations of the Fe-N-C/Fe₃C, Fe-N-C. The dashed line at 0 eV indicates the Fermi level (the inset is a charge density difference diagram). (C) The schematic illustration of Na⁺ storage mechanism of Fe-N-C/Fe₃C@HCNs, and structure changes during discharge/charge process. Reproduced with permission from Ref.^[60], © Tsinghua University Press 2021. (D) Fe-NPSA@NC and (E) Fe-ACSA@NC (the colors yellow and blue represent the increase and decrease of charge density, respectively). (F) OH⁻ adsorption energy as a function of Bader charge. Reproduced with permission from Ref.^[84], © WILEY-VCH Verlag GmbH & Co. KGaA, Weinheim 2021. (G) The schematic illustration for the synthesis of Fe/Fe_xC@Fe-N-Cs electrocatalyst via "MOF-on-MOF" oriented assembly and the confinement conversion procedures. The free energy diagram for O₂ reduction on (H) Fe-N₄ and (I) Fe-N₄-Fe₁₀ under different potentials. Reproduced with permission from Ref.^[85], © Elsevier Ltd. 2023.

carbonization, respectively. The cubic morphologies of Fe atomic cluster functionalizing dispersed metal single-atoms (Fe-ACSA@NC) and Fe NPs functionalizing dispersed metal single-atoms (Fe-NPSA@NC) were confirmed *via* structural characterization. Using XPS spectra and Fourier transform k³-weighted Fe K-edge EXAFS spectra analysis of Fe, the coordination modes of Fe in the sample were found to be Fe-Fe and Fe-N, corresponding to Fe nanoclusters and Fe-N-C sites, respectively. By comparing the differential charge density plots of Fe-ACSA@NC and Fe-NPSA@NC, it was found that the decoration of nano-sized Fe clusters induced electron redistribution around the Fe-N active site [Figure 4D and E]. The electrons around the metal Fe sites were transferred to the adjacent carbon matrix, making the Fe sites more positive and weakening the OH⁻ adsorption energy. Analysis of the relationship between the Bader charge and OH⁻ adsorption energy [Figure 4F] revealed that the OH⁻ adsorption energy has a linear relationship with the Bader charge; Fe-NPSA@NC with a Bader charge of 0.64 V shows the strongest OH⁻ adsorption energy. In contrast, Fe-ACSA@NC with a higher Bader charge showed the weakest OH⁻ binding tendency, promoting the desorption of OH⁻ and thus preserving the active site for subsequent reactions.

Similar to the above work, Chen *et al.* prepared a spindle-like Fe/Fe_xC@Fe-N-Cs [Figure 4G]^[85]. The Gibbs free-energy diagrams of the four-electrons pathway of ORR on the Fe-N₄-Fe₁₀ models are shown in Figure 4H. When the external voltage is 0 (U = 0), the free energy of both models appears downhill,

indicating that the reaction is exothermic and spontaneous. The Fe-N₄-Fe₁₀ model exhibits a lower overpotential ($\eta = 0.27$ V) in the RDS than that of the Fe-N₄ structure, which has a more efficient ORR activity on Fe-N₄-Fe₁₀. Fe-N₄-Fe₁₀ has a higher half-wave potential ($E_{1/2} = 0.81$ V), implying that its ORR activity is higher [Figure 4I]. Due to the presence of Fe₁₀, a considerable amount of electron is transferred, which significantly affects the ORR process (especially OOH[•] production), the catalytic effect occurs due to this activity.

Strong electron coupling

In SMACs, the presence of clusters directly affects the distribution of electrons on the catalyst surface. Charge distribution occurs throughout the *d*-band center of the catalyst, and its effect on the catalytic process cannot be ignored. Yao *et al.* used F127 as a surfactant for the self-assembly of 3-aminophenol and hexamethylenetetramine in a solution. They then conducted annealing carbonization to obtain Ru SA coupling with ultrafine nanoclusters on hierarchical porous N-doped carbon (NMC-Ru_{SA+NC})^[86]. DFT and experimental results reveal the existence of a strong electron coupling effect between Ru SA and nanoclusters. As shown in Figure 5A, by comparing the positions of the *d*-band centers of RuN₄, Ru cluster + RuN₄ and Ru cluster, the strength of adsorption and desorption of Ru cluster + RuN₄ reaches a balance. The adsorption capacity of RuN₄ is too strong, whereas the adsorption capacity of the Ru cluster is too weak. The calculated energy barrier (ΔG_{H^+}) for HER and water splitting are shown in Figure 5B and C, respectively. Among all the models, RuN₄ + Ru clusters have the lowest H⁺ adsorption energy (0.026 eV), indicating that the generated strong electron coupling effect can promote H⁺ desorption to produce hydrogen. In addition, the coupled RuN₄ + Ru cluster has a low energy barrier of 0.03 eV, indicating that the coupled RuN₄ site and Ru nanocluster can achieve rapid hydrolysis splitting, thus improving HER catalytic activity. Ru was previously used as a catalyst for HER^[87]. One-step pyrolysis was conducted on a mixture comprising porous N-doped carbon and Ru precursor (RuCl₃•H₂O)^[88]. DFT calculation results show that the electronic structure of RuN₄ can be adjusted by nearby Ru cluster, optimization of reactants, and the adsorption ability of reaction intermediates (OH[•] or H⁺), which significantly improved the activity of alkaline HER [Figure 5D]. In general, due to the strong electron coupling between Ru cluster and RuN₄, nearby Ru cluster will reduce the adsorption strength of RuN₄ on [•]OH, resulting in the rapid desorption of [•]OH at the active site and providing more active sites for the adsorption and recombination of active hydrogen [Figure 5E].

Spin-state regulation

Regulation of spin states has recently played a vital role in the development of catalysts^[89]. Reasonable spin states can greatly improve catalytic activity^[90-93]. Wei *et al.* synthesized an unprecedented ORR catalyst consisting of Pd nanoclusters (Pd_{NC}) and Fe single-atoms (Fe-N-C/Pd_{NC}) *via* the dual-confinement effect of ZIF-8^[94]. The XAS spectra show that the valence state of Fe species in Fe-N-C/Pd_{NC} and Fe-N-C is between FePc(II) and Fe₂O₃. The D1, D2 and D3 peaks in ⁵⁷Fe Mossbauer spectra belong to low spin (LS), media spin (MS), and high spin (HS), respectively. Relative to Fe-N-C, the D2 peak in Fe-N-C/Pd_{NC} increased from 19.64% to 40.32%. The strong interaction between Fe_{SA} and Pd_{NC} effectively modifies the electronic structure of Fe, the d_{z²} orbit is perpendicular to the Fe-N-C plane, and the original empty d_{z²} orbit of LS Fe (II) becomes a partially occupied orbit in the MS structure, which can effectively adjust the orbital overlap with the oxygen-containing intermediate, such that Fe-N-C/Pd_{NC} has high catalytic activity. With Pd_{NC} loading, the electron transfer from Fe SAs to Pd_{NC} leads to the redistribution of Fe 3*d*-orbital electrons [Figure 6A]. Further details of different orbitals show that this mainly originates from the increasing spin state of Fe d_{z²} orbital [Figure 6B]. Fe-N-C/Pd_{NC} exhibits a high E_{1/2} of 0.94 V in 0.1 M KOH, indicating that Fe-N-C/Pd_{NC} has a better ORR performance [Figure 6C]. As shown in Figure 6D, spin density diagrams of Fe-N-C and Fe-N-C/Pd_{NC} revealed the reason of its enhanced ORR activity. Fe sites with higher spin-states in

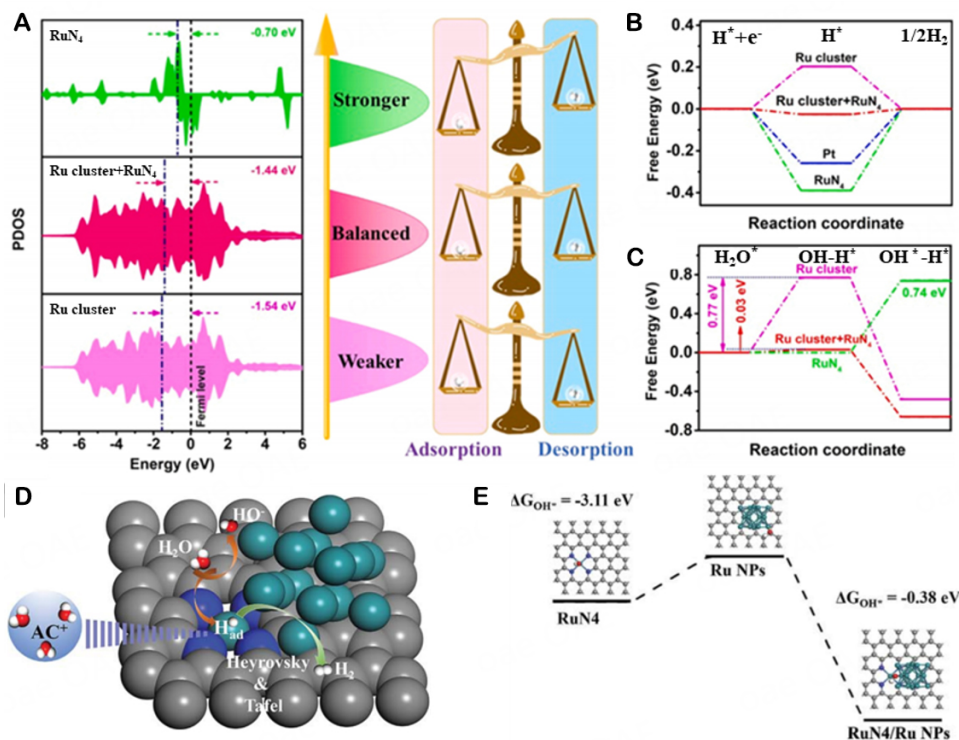


Figure 5. (A) Projected density of states (PDOS) of Ru on the above three Ru systems and the schematic illustration between the *d*-band centers and adsorption-desorption abilities of HER intermediates. (B) Comparison of ΔG_{H^+} of HER on RuN₄, Ru cluster, Ru cluster+RuN₄ and Pt system. (C) The calculated energy barrier for water splitting on RuN₄, Ru cluster and Ru cluster+RuN₄ system. Reproduced with permission from Ref. [86], © Elsevier Ltd. 2022. (D) Schematic of the alkaline HER mechanism for RuN₄/Ru NPs. Gray atoms, blue atoms, cyan atoms, white atoms, and red atoms represent C, N, Ru, H, and O elements. (E) Adsorption energies of the above three Ru models for OH group (OH^{*}). Reproduced with permission from Ref. [88], © The Royal Society of Chemistry 2019.

Fe-N-C/Pd_{NC} create wider spin-related channels, facilitating charge and electron transport during ORR. The original vacant *d*_z² orbital becomes a partially occupied orbital in the MS structure, which can effectively regulate the orbital overlap with the oxygenated intermediate. Correspondingly, the Tafel plot in the higher spin-state Fe-N-C/Pd_{NC} has a lower Tafel slope and, thus, higher reaction kinetics [Figure 6E].

To regulate the spin-states of the active center of the catalyst, Liu *et al.* developed an axial Fe-O-Ti ligand-regulated spin-state transition strategy to improve the ORR activity of the Fe sites^[95]. By bridging Fe SAs to Ti₃C₂T_x, FeN₃O-O-Ti was obtained. Compared with FeN₃O, the formation of FeN₃O-O-Ti significantly increased the amount of charge transfer. Figure 6F shows the increase in the magnetic moment of the Fe site from 1.51 to 3.52 μB, proving that the spin state of the site was from LS to MS, which greatly improved the adsorption energy with O₂ (ΔE_{ads}). In contrast, compared with the calculated PDOS of the Fe 3*d* orbital [Figure 6G], the *d*-band center of FeN₃O-O-Ti was further away from the Fermi level. Thus, the adsorption energy of the oxygenated intermediate could be appropriately adjusted, which is crucial for the ORR process. This conclusion is also supported by the free-energy calculations for the ORR process. FeN₃O must overcome a large energy barrier to form OOH^{*} [Figure 6H].

Electronic metal-support interaction

The electronic metal-support interaction (EMSI) mechanism is based on the metal-support interaction (MSI)^[96-98]. As the support height increases, the EMSI decreases and leads to a significant difference between the atoms at the top and bottom of the nanoclusters (known as tip effect, TE)^[99-103]. The local electric field

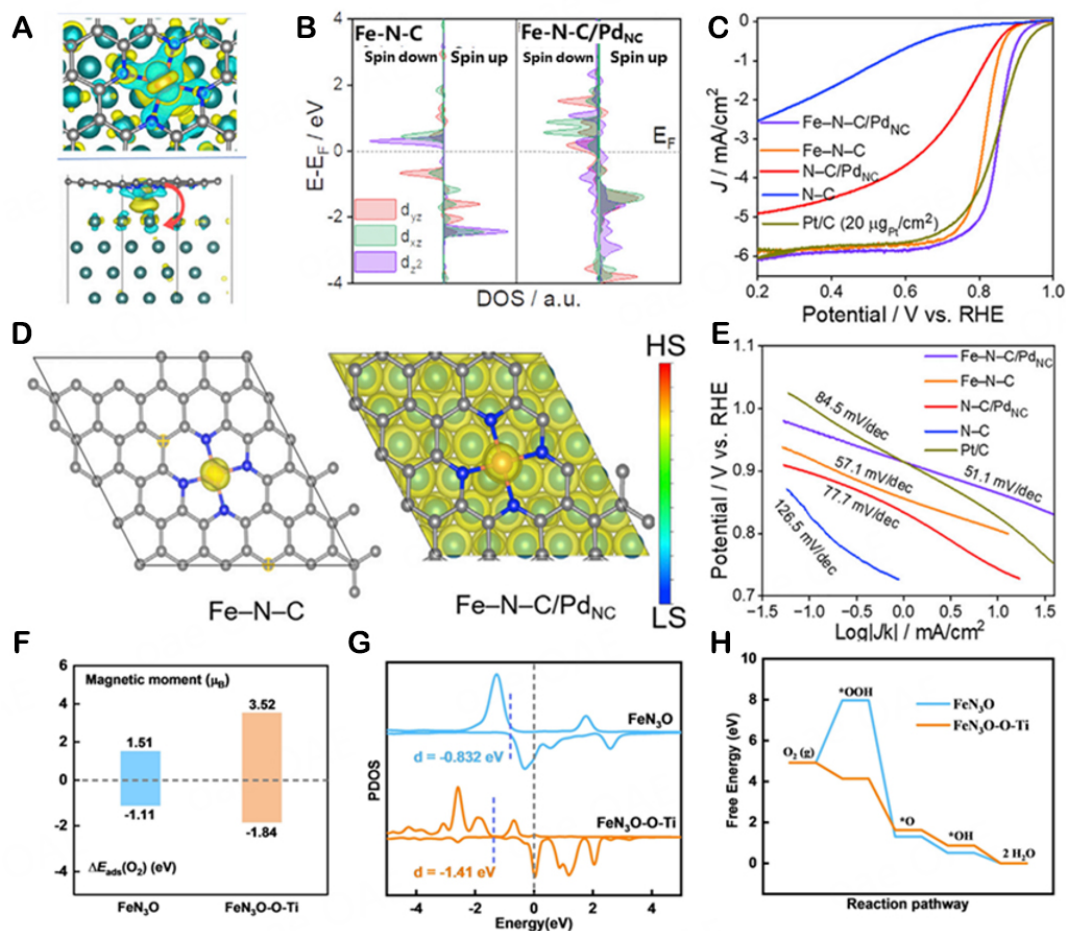


Figure 6. (A) The charge density difference of Fe-N-C/Pd_{NC} (top: top view; bottom: front view. The yellow and cyan regions represent electron accumulation and depletion, respectively). (B) Projected DOS diagrams of Fe-N-C and Fe-N-C/Pd_{NC}. (C) ORR polarization curves measured on RDE in O₂-saturated 0.1 M HClO₄ electrolyte for different catalysts. (D) Spin density diagrams of Fe-N-C and Fe-N-C/Pd_{NC} (the isosurface is 0.1 a.u.). (E) Tafel plots of catalysts. Reproduced with permission from Ref. [94], © Elsevier Ltd. 2022. (F) Calculated relationship between μ_B and ΔE_{ads}(O₂) of FeN₃O and FeN₃O-O-Ti. (G) The PDOS of Fe 3d orbital for FeN₃O and FeN₃O-O-Ti and (H) The free energy changes for ORR. The blue dotted lines denote the d-band centers, while the gray dotted line denotes the Fermi level. Reproduced with permission from Ref. [95], © WILEY-VCH Verlag GmbH & Co. KGaA, Weinheim 2022.

from the tip promotes mass transfer. In addition, the tip often plays an important role in the catalytic reaction due to the synergistic effect of the enhanced electric field effect and the local electric field effect. This results in a suitable adsorption strength of the reversible intermediate. EMSI can be used as a tool to regulate the electronic structure of the metal active site. EMSI is usually so strong that the efficiency of the active site is determined by the metal center and adjacent atoms. It has a flexible electronic environment and a high electron transfer rate; however, it has high adsorption energy and energy barrier.

The size of the cluster greatly affects the charge distribution on the catalyst surface. The smaller the cluster size, the more significant the charge redistribution in the matrix^[104]. Therefore, the surface charge distribution of the cluster must be maintained within an appropriate range of reaction by controlling the cluster size. Yang *et al.* designed an IrO₂ sub-nano cluster catalyst supported by titanium carbide NPs (Ir_n-TiC)^[105]. By regulating the TE and the electronic structure of the coordinatively unsaturated O atom, the excessive EMSI of Ir SACs(Ir₁-TiC) can be reduced to achieve an efficient chlorine evolution reaction. By adjusting the TE strength of the catalyst, the efficiency of titanium-supported subnano IrO₂ clusters

improved compared with that of the atomic Ir clusters, indicating the significance of modified electron interaction. The crystal orbital Hamilton population (COHP) of the interaction between the Ir atoms of different heights and the Ti atoms on the surface of the Ir_n-TiC were shown in [Figure 7A](#). Strong peaks appear at -5.5 and -7.8 V, which correspond to the 5*d* orbit of Ir and 3*d* orbit of Ti, respectively. However, with an increase in the cluster height, the intensity of the two peaks decreases and shifts to a higher energy level, indicating effective regulation of TE. By comparing the electron localization function of the Ir₁-TiC and Ir_n-TiC [[Figure 7B](#)], it can be found that when the isolate Ir sites are supported by the TiC (Ir₁-TiC), an electrovalent bond is almost formed between Ir and TiC. For Ir_n-TiC, although the bottom atom and carrier have strong EMSI, the top Ir atom and oxygen atom are weakly affected, with stronger TE; this indicates that electrons are more easily transferred between active centers. The charge density difference of the Ir₁-TiC, as shown in [Figure 7C](#), can also prove that the EMSI in Ir₁-TiC is strong. In summary, the number of electron transfers decreases as the distance from the support increases. The distance between the Ir atoms on the oxidized sub-nano cluster catalysts and the TiC modulates the TE so that different tracks overlap to the appropriate level.

Similarly, when the cluster size is fixed, the atomic cluster will be regulated by the charge redistribution from the cluster. Zhou *et al.* developed Mo SAs@1T-CrS₂ nanoflake through the simple synthesis of laser-molecular beam epitaxy (L-MBE) technology^[106]. As shown in [Figure 7D](#), the Mo atom can be successfully anchored to the metal substrate of 1T-CrS₂ nanosheet by S atom under the resulting Mo plasma, which can induce TE by local electric field. Fourier transform of the k³-weighted Mo K-edge of the EXAFS spectra can prove that the coordination form for Mo is Mo-S. Mo SAs@1T-CrS₂ shows excellent electrocatalytic performance and ultra-high stability, which is superior to 1T-CrS₂. The schematic of electric field distribution of Mo SAs@1T-CrS₂ nanoflake is shown in [Figure 7E](#). This figure shows that the charge density around Mo atom increases, enhancing the coupling of H⁺. By comparing the calculated free-energy diagram of HER at the equilibrium potential for Mo SAs@1T-CrS₂, 1T-CrS₂, and Pt, it can be found that the ΔG_{H⁺} of Mo SAs@1T-CrS₂ is lower than that of 1T-CrS₂ [[Figure 7F](#)]. Thus, it is theoretically proved that atomic Mo on the 1T-CrS₂ substrate plane is the active sites of efficient HER.

In summary, most of the research on changes in charge transfer, spin state, or EMSI caused by electric charge distribution comes from theoretical calculations. It is worth noting that SMACs, as a relatively complex catalytic system, may contain many more active sites than the structures calculated by researchers. Therefore, it is limited to prove the active site and the catalytic reaction process at the active site only by calculations. To support the theoretical calculation results, a more accurate characterization of the charge transfer/electron coupling/spin states is needed as experimental evidence. For example, the number of unpaired electrons of the material can be detected by electron paramagnetic resonance (EPR), and the magnetic moment of the material can be detected by vibrating sample magnetometer (VSM) to evaluate the change of spin state, *etc.* This is also another requirement for the characterization of materials.

Mutual assistance of single metallic atom/clusters electrocatalysts

SMACs contain multiple reaction sites; however, not all sites are involved in the catalytic process^[107]. This does not mean that the presence of these phases is meaningless; on the contrary, it may be crucial for the actual catalytic sites. The interaction between SMA and metal clusters can regulate the electronic and geometric structure of the active sites, change the adsorption energy of intermediates, and ultimately affect the reaction pathway. It is one of the advanced design strategies for synthesizing high-performance catalysts, combining the advantages of different catalytic sites and exploiting the characteristics of each metal active site to improve the catalytic efficiency. Researchers have recently developed catalysts containing different catalytic actions, providing a platform for understanding the mutual assistance within catalysts at a molecular level^[14].

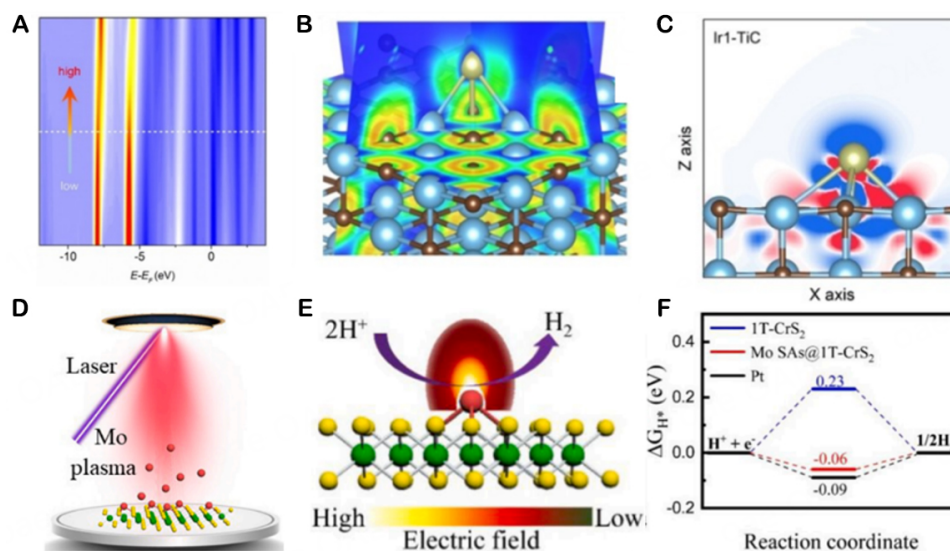


Figure 7. (A) The crystal orbital Hamilton population of the interaction between the Ir atoms of different heights and the Ti atoms on the surface of the Ir₁-TiC. (B) The electron localization function of the Ir₁-TiC. (C) The charge density difference of the Ir₁-TiC. (D) Synthesis schematic of Mo SAs on a 1T-CrS₂ nanoflake by L-MBE. Reproduced with permission from Ref. ^[105], © WILEY-VCH Verlag GmbH & Co. KGaA, Weinheim 2022. (E) Schematic of electric field distribution of Mo SAs@1T-CrS₂ nanoflake. (F) The calculated free-energy diagram of HER at the equilibrium potential for Mo SAs@1T-CrS₂, 1T-CrS₂ and Pt. Reproduced with permission from Ref. ^[106], © Elsevier Ltd. 2021.

Single atom assisted cluster site

SMA carriers consist of multiple elements. The coordination environment at SMA sites is diverse and difficult to control, making it difficult to achieve specific bonding reactions (e.g., C-C coupling). As shown in Figure 8A, Ou *et al.* catalyzed C-C coupling by loading Au SAs on a red phosphorus (RP) catalyst (Au₁/RP)^[43]. RP is a carrier comprising a single element with a homogeneous structure, lower electronegativity, and better CO₂ absorption. Electron-rich phosphorus atoms near the Au single nucleus can serve as the active site for CO₂ activation. The Au SA can effectively lower the energy barrier for C-C coupling and promote the reaction kinetics of C₂H₆ formation. As shown in Figure 8B, the peak is located at 1.8 Å, which corresponds to Au-P coordination, and the coordination number of the Au SA of the Au₁/RP catalyst is about 2. A schematic of Au₁/RP catalyst for C-C coupling is shown in Figure 8C. The Au SA facilitates the desorption and migration of C₁ intermediates at the P reactive site, followed by C-C coupling at another P site. The poor durability of Pt-based NPs dispersed on carbon black is a major challenge for long-life PEMFCs applications. Xiao *et al.* prepared Fe-N-C catalysts *via* one-step pyrolysis, followed by Pt loading using liquid phase method to obtain Pt/Fe-N-C^[65]. The coordination forms of Pt and Fe in the catalyst can be obtained by Pt L₃-edge with the Pt foil and Pt/C-TKK references and Fe K-edge with Fe-N-C and Fe foil standards, respectively. DFT calculations reveal that Pt/Fe-N-C has the lowest binding energy to the carrier (-4.60 eV), followed by Pt/N-C (-3.86 eV) and Pt/C (-2.84 eV), indicating that Fe-N-C provides the strongest carrier. Figure 8D shows the -pCOHP and reveals that the formation of oxides is mitigated by modulating the electronic structure. Stronger metal-substrate interactions, along with lower metal dissolution rates and highly stable support, result in robust formation compared to Pt/Fe-N-C. The remaining two antibonding states are less populated. By adjusting the electronic structure of the Pt cluster, the Fe-N-C support weakens the O[•] adsorption strength on the Pt cluster (the *d*-band center of Pt shifts downward from -2.16 eV (Pt/C) to -2.28 eV. The negative shift of the *d*-band center weakened the interaction of Pt/Fe-N-C with the adsorbent O[•]), thus mitigating the formation of Pt oxides, which may be another reason for the lower dissolution rate of Pt.

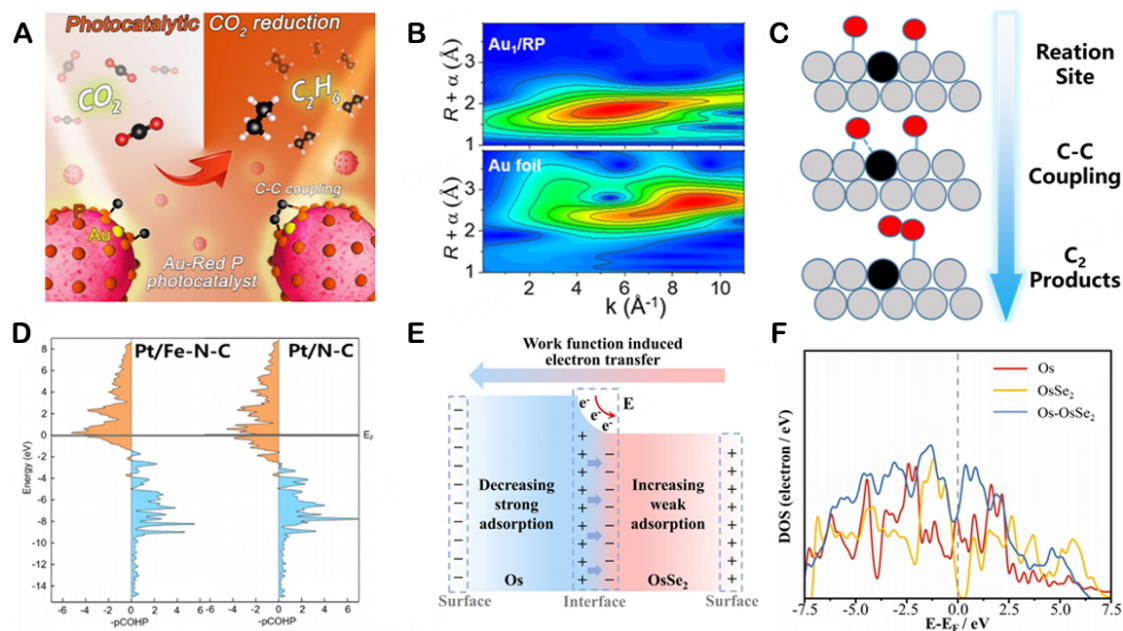


Figure 8. (A) Interface-assisted catalytic C-C Coupling of Au single-atoms over red phosphorus. Photocatalytic reduction of CO_2 to ethane. (B) Wavelet-transformed k^3 -weighted EXAFS spectra of samples. (C) Schematic illustration of Au₁/RP for C-C coupling. Reproduced with permission from Ref. [43], © American Chemical Society 2022. (D) Optimized structures of Pt/Fe-N-C, Pt/N-C, and Pt/C, along with projected crystal orbital Hamilton population analysis. Reproduced with permission from Ref. [65], © American Chemical Society 2022. (E) Charge transfer process in Os-OsSe₂. (F) The DOS of Os, OsSe₂, and Os-OsSe₂. Reproduced with permission from Ref. [4], © WILEY-VCH Verlag GmbH & Co. KGaA, Weinheim 2022.

Work function (WF), as a parameter reflecting electron escape ability, is widely used to reveal the electron transfer process in heterogeneous catalysts. Chen *et al.* constructed Os-OsSe₂ heterostructures with molten salt-assisted synthesis strategy, in which the WF determined the built-in electric field and the direction of charge transfer [Figure 8E]^[4]. As the cheapest metal in the Pt group, Os has an extremely strong binding energy to H⁺; thus, it cannot be used as a catalyst for HER. The built-in electric field drives the transfer of electric charges from Os to OsSe₂ due to the differences in WFs on both sides of the Os-OsSe₂ heterogeneous structure. The resulting interfacial equilibrium significantly weakened the adsorption strength of Os to H⁺. Os-OsSe₂ had the highest density of states near the Fermi level, as shown in Figure 8F. Similarly, SMACs charge transfer resulting from differences in WFs is the internal driving mechanism of SMACs catalysts.

Cluster assisted single atom site

So far, Fe-N-C is one of the widely used catalysts^[108]. However, due to thermodynamic instability, Fe atoms tend to migrate and coalesce into NPs during pyrolysis^[109]. This makes high loading of atomic Fe catalyst difficult. However, the presence of clusters does not only have negative effects on Fe-N-C catalyst^[108]. Ao *et al.* used covalent organic frameworks (COFs) as precursors to prepare an efficient ORR electrocatalyst with both atomic clusters and SAs (Fe_{AC}@Fe_{SA}-N-C)^[110]. The free-energy path was calculated as shown in Figure 9A by comparing the RDS ($\text{O}_2 \rightarrow \text{OOH}^{\cdot}$) of Fe_{AC}@Fe_{SA}-N-C and Fe_{SA}-N-C. The RDS of Fe_{AC}@Fe_{SA}-N-C is much smaller than that of Fe_{SA}-N-C, implying that it is more dominant in terms of reaction kinetics. Similarly, a comparison of the calculated overpotentials of the ORR for the Fe₁@Fe_{SA}-N-C, Fe₁₃@Fe_{SA}-N-C, Fe_{NP}@Fe_{SA}-N-C, and Fe_{SA}-N-C models shows that the overpotential of Fe₁₃@Fe_{SA}-N-C is smaller than that of Fe_{SA}-N-C. This indicates that the reaction can occur at a much lower potential [Figure 9B]. The half-wave potential of Fe_{AC}@Fe_{SA}-N-C is 0.912 V [Figure 9C], which exceeds that of the non-platinum group metal

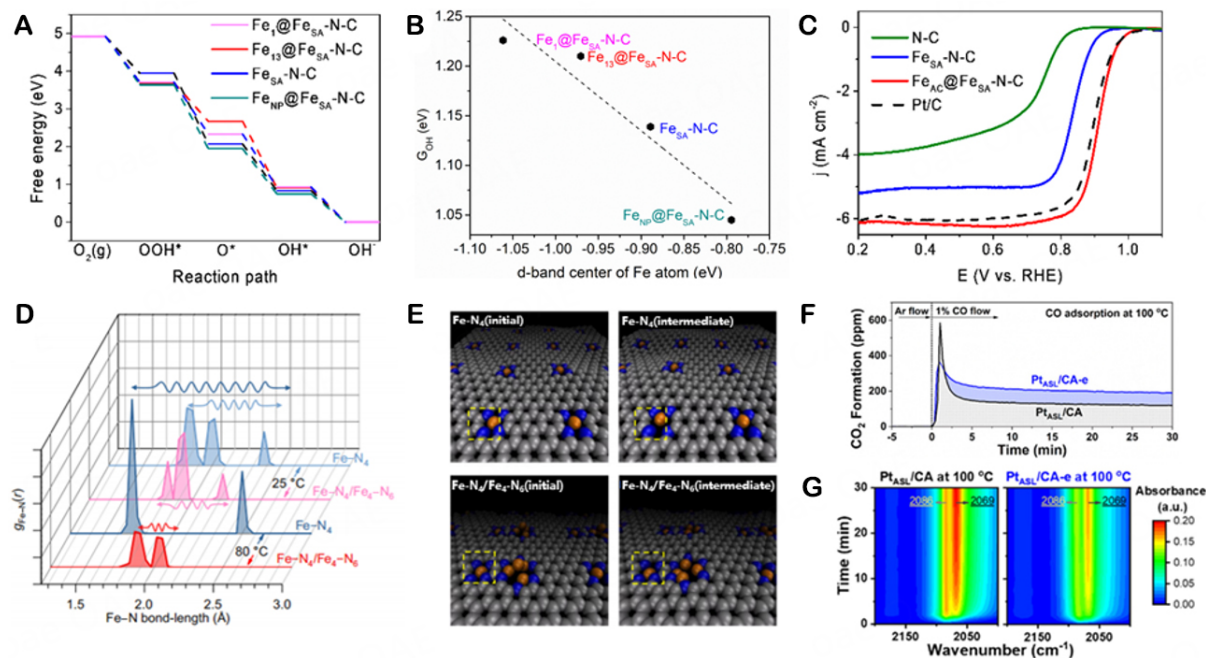


Figure 9. (A) Free-energy path and (B) calculated overpotentials of the ORR for the $\text{Fe}_1\text{@FeSA-N-C}$, $\text{Fe}_{13}\text{@FeSA-N-C}$, FeNP@FeSA-N-C , and FeSA-N-C models. (C) LSV curves of FeAC@FeSA-N-C , FeSA-N-C , N-C , and Pt/C in O_2 -saturated 0.1 M KOH solution with a rotation rate of 1,600 rpm and a sweep rate of 10 mV s^{-1} . Reproduced with permission from Ref. ^[110], © American Chemical Society 2019. (D) Fe-N radical distribution function profiles of the Fe-N_4 moiety in the models of bare Fe-N_4 and $\text{Fe-N}_4/\text{Fe}_4\text{-N}_6$ at 25 and 80 °C. Wavy arrows are used to indicate the amplitude of Fe-N bond-length fluctuation. (E) Snapshots of Fe-N_4 and $\text{Fe-N}_4/\text{Fe}_4\text{-N}_6$ obtained from MD simulations at 80 °C. The initial configuration (left) and an intermediate state (right) are provided to show the elongation of the Fe-N bond as marked by the yellow box. (F) Time-resolved CO_2 formation after exposure to continuous CO flow and (G) *in situ* DRIFTS of CO adsorption. Reproduced with permission from Ref. ^[112], © American Chemical Society 2022.

catalysts. These studies not only confirm the importance of Fe-N_4 sites but also show that additional Fe atoms/clusters, e.g., Fe_1 and Fe_{13} , can play important roles in enhancing the catalytic activity of Fe-N_4 sites, even if these atomic clusters are not reactive sites themselves. The introduction of clusters can improve the catalytic activity of the original SMA sites and the cluster catalysts.

Achieving enhanced catalytic effect by inhibiting transition metal leaching as well as balancing stability and activity are crucial for practical applications of proton-exchange membrane fuel cells. Wan *et al.* used protonated N-doped carbon substrates to produce moderate coordination strengths for metallic elements during heat treatment, thereby introducing Fe clusters and thus achieving uniform dispersion of Fe_{SA} and Fe_{NP} ^[111]. Experimental and theoretical evidence shows strong electronic interactions between Fe_{SA} and Fe_{NP} due to the smooth electron transfer pathway and very short interaction distances. The RDS of ORR on Fe-N_4 is the formation of OH^* ($\text{O}^* + \text{H}^+ + \text{e}^- = \text{OH}^*$), with an energy barrier of 0.53 eV. When Fe_{NP} is introduced, $\text{Fe-N}_4/\text{Fe}_4\text{-N}_6$ exhibits strong adsorption to OH, allowing a permanent OH ligand to be grafted onto Fe-N_4 . Fe clusters can introduce OH ligands and lower the ORR energy barrier, thus increasing the activity of Fe-N_4 sites. If a Fe-N bond is long and widely distributed, it is prone to fracture. As the Fe-N radical distribution function profiles of the Fe-N_4 moiety shows in Figure 9D, at room temperature, the $g_{\text{Fe-N}}(r)$ of Fe-N_4 showed three peaks in the range of 1.82–2.38 Å due to the thermal vibration of Fe-N bonds. After the addition of Fe clusters, the length distribution of Fe-N bonds narrowed to 1.82–2.22 Å, indicating that these bonds are stable. Previous studies predicted that the vibrational frequency of metal clusters increases with decreasing cluster size up to diatomic molecules. Therefore, the researchers reasonably hypothesized that the incoherent vibrations of Fe_{NP} and Fe_{SA} are responsible for the decrease in the Fe-N

bond amplitude. Fe_{NF} produces a “pinning effect” that suppresses the thermal vibrations of the Fe-N_4 sites, thus reducing their tendency to demetallize [Figure 9E].

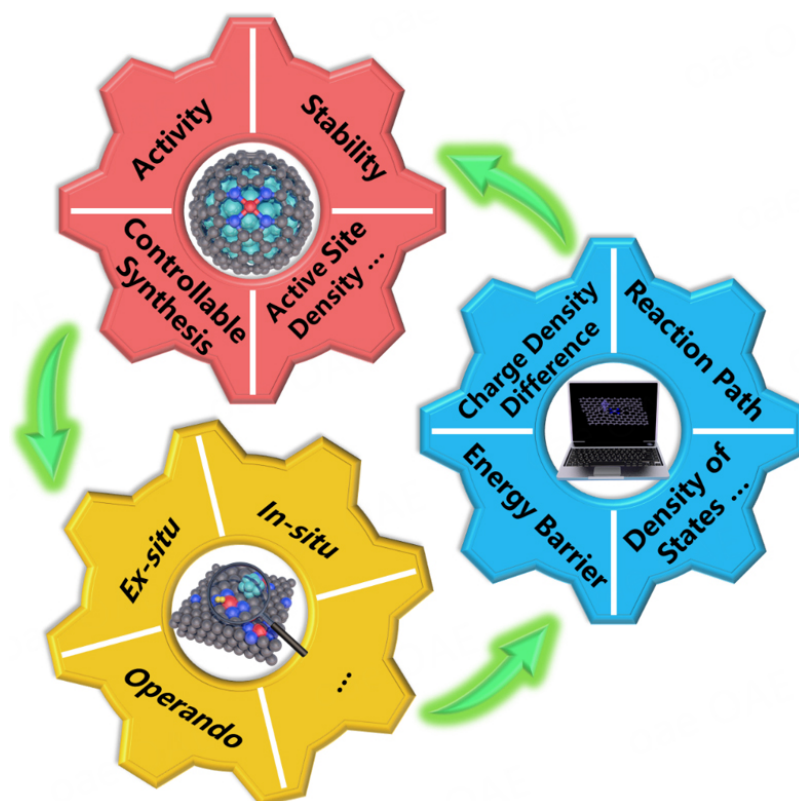
Xie *et al.* succeeded in enriching defective $\text{CeO}_2\text{-Al}_2\text{O}_3$ carriers with different local coordination environments on the surface for atomic Pt (Pt_i) and Pt atomic single-layer (Pt_{ASL}) and Pt multilayer cluster (Pt_c) catalysts with 100% metal dispersion and precisely controlled local coordination environments using a surface defect enrichment strategy^[112]. To determine the reactive oxygen species and better understand the advantages of embedded Pt_{ASL} ($\text{Pt}_{\text{ASL-e}}$), the *in-situ* DRIFT study at 100 °C to monitor the reaction of CO with oxygen in $\text{Pt}_{\text{ASL}}/\text{CA}$ and $\text{Pt}_{\text{ASL}}/\text{CA-e}$ catalysts [Figure 9F and G]. Compared with the intense CO formation peak observed on $\text{Pt}_{\text{ASL}}/\text{CA}$, a lower CO formation peak was observed on $\text{Pt}_{\text{ASL}}/\text{CA-e}$, indicating that less surface oxygen is present on $\text{Pt}_{\text{ASL}}/\text{CA-e}$. The oxygen vacancies of $\text{CeO}_2\text{-Al}_2\text{O}_3$ effectively promote the synthesis of Pt materials at different atomic levels, bringing positive effects for the subsequent adsorption and oxidation of CO.

CONCLUSION AND OUTLOOK

In most single metallic atom/clusters (SMACs) catalysts, single metallic atom (SMA) sites are the main active sites, while the presence of clusters often serves as a matrix. Precise regulation of the coordination environment of the single metallic atom and the change in electronic structure induced by the introduction of clusters, as well as appropriate regulation of SMACs interactions, are important ways to optimize the catalytic activity of SMACs. Although SMA catalysts have outstanding advantages in terms of improving atomic utilization and reducing cost, their catalytic activity and stability cannot be guaranteed if the structural stability of single atoms cannot be ensured. Therefore, SMAs and clusters are combined to obtain advanced catalysts with high catalytic activity and stability as well as improved atomic utilization.

In this review, SMACs based on their synthesis methods and catalytic reaction mechanisms. The mechanisms by which various SMACs play a role in the catalytic process and the influence of these mechanisms on their catalytic performance are discussed along with the synergistic effect of carriers and clusters in the catalytic process. Machine learning is gaining popularity in the field of catalysis. Artificial intelligence, which combines Big Data and machine learning for catalyst selection and design, has significantly accelerated the related research. A machine learning framework was used to improve computational speed and obtain catalysts with high catalytic activity. The as-obtained catalysts were matched with the experimental results to create an efficient catalyst design^[113,114]. SMACs are being extensively researched. However, due to limitations in characterization techniques, their electronic structure and reaction dynamics cannot be monitored, which results in an insufficient understanding of their reaction kinetics. To understand the reaction mechanism and kinetics of SMACs and to synthesize SMACs with high catalytic activity, more accurate *in-situ* characterization techniques and computational simulations are required. Thus, many crucial challenges have to be addressed [Scheme 3].

(I) Synthesize of SMACs with high efficiency and stability. The technology to synthesize SMACs is not yet mature and is more challenging than those used for the synthesis of SMAs and cluster catalysts. Computational models can be used for catalysis; however, using theoretical models due to their limited precision and controllability for material synthesis. Strategies that enable accurate synthesis of SMACs, such as ALD, are expensive and involve matrix selection; thus, they cannot be readily applied on a large scale. A universal and accurate synthesis strategy is required for the development of synthesis methods such as the loading of metal clusters with controllable sizes onto different SMA matrixes or the loading of single atoms with controllable site density onto different metal clusters. Notably, metal cluster loading and morphology-controllable synthesis are promising methods for catalyst development.



Scheme 3. Proposed future directions towards advanced single metallic atom/clusters catalyst in energy electrocatalysis.

(II) Identification of truly active sites in SMACs and dynamic changes during catalysis as well as the analysis of the formation and disappearance of reaction intermediates: Advanced characterization methods are used to simultaneously determine the active sites and monitor catalyst transformation under working conditions. The combination of *in situ* and operando structural characterization (e.g., *in-situ* Mössbauer spectroscopy, online mass spectrometry, ultrafast spectroscopy, and operando XAS) is an important tool for understanding the activation and deactivation of catalyst sites. For example, in actual catalytic studies, the formation, transformation and disappearance of reaction intermediates in the system can be clearly understood by *in-situ* FTIR. At the same time, *in-situ* Raman can be used to characterize the change in catalyst composition at the same time. Combining the two results gives insight into the catalytic process. This is necessary to understand the mechanism of the reaction. Future research should focus on developing complete and functional *in-situ* and operando instrumentation for complex reaction systems.

(III) Artificial intelligence is of guiding significance to the design of catalysts. As mentioned above, the existence of big data can analyze current research hotspots, but it is still difficult for researchers to accurately choose these huge data. Through artificial intelligence training, the research hotspot can be sorted out and the structure of catalyst can be predicted. On this basis, combined with the interest of researchers, the catalyst is screened. In conclusion, using artificial intelligence for prediction and pre-selection is an interesting option for reducing researchers' workload and improving research efficiency.

(IV) Simulation of the complexity and dynamics of catalytic systems using computational modeling. Similar to machine learning, theoretical calculations can guide catalyst design, and the calculation process is not constrained by practical conditions, so impractical solutions can be ruled out in advance. However,

theoretical calculation results may not be realized. On the one hand, the synthesis of prefabricated catalysts may fail due to limited resources; on the other hand, the validity of theoretical calculations can only be proven when the results are verified *via* structural, morphological, and physicochemical characterization techniques. Therefore, reasonable theoretical calculations can distinguish catalysts with different structures to determine reaction pathways and active reaction sites.

Understanding and developing multiatom cluster catalysts is fraught with challenges and opportunities. Combining SMAs and metal clusters is critical to the development of new-generation catalyst systems. SMACs are used not only in electrocatalysis but also in thermal and environmental catalysis. Its potential in pollution control, renewable energy, carbon neutrality, and other industries should help alleviate global energy and environmental problems. In the future, efficient SMACs will be developed to optimize industrial production processes, reduce production costs, and prevent pollution.

DECLARATIONS

Authors' contributions

Proposed the topic of this review: Zhang JN

Prepared the manuscript: Wei Y, Xia H

Collectively discussed and revised the manuscript: Wei Y, Xia H, Yan W, Zhang JN

Availability of data and materials

Not applicable.

Financial support and sponsorship

This work was supported by the National Natural Science Foundation of China (U22A20107) and the Distinguished Young Scholars Innovation Team of Zhengzhou University (32320275). The Science and Technology R&D Program Joint Fund Project of Henan Provincial (222301420001), and Postgraduate Education Reform Project of Henan Province (2021SJGLX093Y).

Conflicts of interest

All authors declared that there are no conflicts of interest.

Ethical approval and consent to participate

Not applicable.

Consent for publication

Not applicable.

Copyright

© The Author(s) 2023.

REFERENCES

1. Armand M, Tarascon JM. Building better batteries. *Nature* 2008;451:652-7. [DOI](#) [PubMed](#)
2. Pomerantseva E, Bonaccorso F, Feng X, Cui Y, Gogotsi Y. Energy storage: the future enabled by nanomaterials. *Science* 2019;366:eaan8285. [DOI](#) [PubMed](#)
3. Xiao Y, Xu R, Xu L, Ding J, Huang J. Recent advances in anion-derived SEIs for fast-charging and stable lithium batteries. *Energy Mater* 2022;1:100013. [DOI](#)
4. Chen D, Lu R, Yu R, et al. Work-function-induced interfacial built-in electric fields in Os-OsSe₂ Heterostructures for Active Acidic and Alkaline Hydrogen Evolution. *Angew Chem Int Ed* 2022;61:e202208642. [DOI](#)
5. Deng J, Ren P, Deng D, Bao X. Enhanced electron penetration through an ultrathin graphene layer for highly efficient catalysis of the

- hydrogen evolution reaction. *Angew Chem Int Ed* 2015;54:2100-4. DOI PubMed
6. Zhu J, Guo Y, Liu F, et al. Regulative electronic states around ruthenium/ruthenium disulphide heterointerfaces for efficient water splitting in acidic media. *Angew Chem Int Ed* 2021;60:12328-34. DOI
 7. Pan F, Jin T, Yang W, et al. Theory-guided design of atomic Fe-Ni dual sites in N,P-co-doped C for boosting oxygen evolution reaction. *Chem Catal* 2021;1:734-45. DOI
 8. Liu S, Li C, Zachman MJ, et al. Atomically dispersed iron sites with a nitrogen-carbon coating as highly active and durable oxygen reduction catalysts for fuel cells. *Nat Energy* 2022;7:652-63. DOI
 9. Wang X, Fu N, Liu JC, et al. Atomic replacement of PtNi nanoalloys within Zn-ZIF-8 for the fabrication of a multisite CO₂ reduction electrocatalyst. *J Am Chem Soc* 2022;144:23223-9. DOI
 10. Xue D, Xia H, Yan W, Zhang J, Mu S. Defect engineering on carbon-based catalysts for electrocatalytic CO₂ reduction. *Nanomicro Lett* 2020;13:5. DOI PubMed PMC
 11. Zhang Y, Gao P, Jiao F, et al. Chemistry of ketene transformation to gasoline catalyzed by H-SAPO-11. *J Am Chem Soc* 2022;144:18251-8. DOI
 12. Garrido-Barros P, Derosa J, Chalkley MJ, Peters JC. Tandem electrocatalytic N₂ fixation via proton-coupled electron transfer. *Nature* 2022;609:71-6. DOI PubMed
 13. Li Z, Deng Z, Ouyang L, et al. CeO₂ nanoparticles with oxygen vacancies decorated N-doped carbon nanorods: a highly efficient catalyst for nitrate electroreduction to ammonia. *Nano Res* 2022;15:8914-21. DOI
 14. Xia H, Zan L, Wei Y, et al. Catalytic effect of carbon-based electrode materials in energy storage devices. *Sci China Mater* 2022;65:3229-42. DOI
 15. Qing G, Ghazfar R, Jackowski ST, et al. Recent advances and challenges of electrocatalytic N₂ reduction to ammonia. *Chem Rev* 2020;120:5437-516. DOI
 16. Zhou L, Chen L, Ding Z, et al. Enhancement of interfacial catalysis in a triphase reactor using oxygen nanocarriers. *Nano Res* 2021;14:172-6. DOI
 17. Liu M, Lei Z, Ke Q, et al. Regulation of hydrogen evolution performance of titanium oxide-carbon composites at high current density with a Ti-O hybrid orbital. *Carbon Energy* 2022;4:480-90. DOI
 18. Chen X, Qiao Z, Hou B, et al. Chiral metal-organic frameworks with tunable catalytic selectivity in asymmetric transfer hydrogenation reactions. *Nano Res* 2021;14:466-72. DOI
 19. Zhang X, Zhu X, Bo S, et al. Identifying and tailoring C-N coupling site for efficient urea synthesis over diatomic Fe-Ni catalyst. *Nat Commun* 2022;13:5337. DOI PubMed PMC
 20. Wan X, Shui J. Exploring durable single-atom catalysts for proton exchange membrane fuel cells. *ACS Energy Lett* 2022;7:1696-705. DOI
 21. Hu J, Xu Q, Wang X, et al. Charge-transfer-regulated bimetal ferrocene-based organic frameworks for promoting electrocatalytic oxygen evolution. *Carbon Energy* 2023;5:e315. DOI
 22. Guo Y, Wang M, Zhu Q, Xiao D, Ma D. Ensemble effect for single-atom, small cluster and nanoparticle catalysts. *Nat Catal* 2022;5:766-76. DOI
 23. Cheng N, Stambula S, Wang D, et al. Platinum single-atom and cluster catalysis of the hydrogen evolution reaction. *Nat Commun* 2016;7:13638. DOI PubMed PMC
 24. Kim J, Yoo JM, Lee HS, Sung Y, Hyeon T. Single-atom M-N-C catalysts for oxygen reduction electrocatalysis. *Trends Chem* 2021;3:779-94. DOI
 25. Tang X, Wei Y, Zhai W, et al. Carbon nanocage with maximum utilization of atomically dispersed iron as efficient oxygen electroreduction nanoreactor. *Adv Mater* 2023;35:e2208942. DOI
 26. Song LN, Zhang W, Wang Y, et al. Tuning lithium-peroxide formation and decomposition routes with single-atom catalysts for lithium-oxygen batteries. *Nat Commun* 2020;11:2191. DOI PubMed PMC
 27. Han L, Cheng H, Liu W, et al. A single-atom library for guided monometallic and concentration-complex multimetallic designs. *Nat Mater* 2022;21:681-8. DOI
 28. Xia H, Qu G, Yin H, Zhang J. Atomically dispersed metal active centers as a chemically tunable platform for energy storage devices. *J Mater Chem A* 2020;8:15358-72. DOI
 29. Tian Z, Zhang Y, Zhu J, Li Q, Liu T, Antonietti M. A reanalysis of the diverse sodium species in carbon anodes for sodium ion batteries: a thermodynamic view. *Adv Energy Mater* 2021;11:2102489. DOI
 30. Kumar K, Asset T, Li X, et al. Fe-N-C electrocatalysts' durability: effects of single atoms' mobility and clustering. *ACS Catal* 2021;11:484-94. DOI
 31. Patniboon T, Hansen HA. Acid-stable and active M-N-C catalysts for the oxygen reduction reaction: the role of local structure. *ACS Catal* 2021;11:13102-18. DOI
 32. Rojas-carbonell S, Artyushkova K, Serov A, Santoro C, Matanovic I, Atanassov P. Effect of pH on the activity of platinum group metal-free catalysts in oxygen reduction reaction. *ACS Catal* 2018;8:3041-53. DOI
 33. Wu Z, Shen J, Li C, et al. Mo₂TiC₂ MXene-supported Ru clusters for efficient photothermal reverse water-gas shift. *ACS Nano* 2022;17:1550-9. DOI
 34. Wang Y, Guo T, Tian Z, Bibi K, Zhang YZ, Alshareef HN. MXenes for energy harvesting. *Adv Mater* 2022;34:e2108560. DOI
 35. Liu H, Jiang L, Khan J, et al. Decorating single-atomic mn sites with FeMn clusters to boost oxygen reduction reaction. *Angew Chem*

- Int Ed* 2023;62:e202214988. DOI
36. Ye C, Zheng M, Li Z, et al. Electrical pulse induced one-step formation of atomically dispersed Pt on oxide clusters for ultra-low-temperature zinc-air battery. *Angew Chem Int Ed* 2022;61:e202213366. DOI
 37. Yang L, Li G, Ma R, et al. Nanocluster PtNiP supported on graphene as an efficient electrocatalyst for methanol oxidation reaction. *Nano Res* 2021;14:2853-60. DOI
 38. Yin H, Xia H, Zhao S, Li K, Zhang J, Mu S. Atomic level dispersed metal-nitrogen-carbon catalyst toward oxygen reduction reaction: synthesis strategies and chemical environmental regulation. *Energy Environ Mater* 2021;4:5-18. DOI
 39. Zhao S, Yin H, Xia H, et al. The assembling principle and strategies of high-density atomically dispersed catalysts. *Chem Eng J* 2021;417:127917. DOI
 40. Wu Z, Zhao Y, Xiao W, et al. Metallic-bonded Pt-Co for atomically dispersed Pt in the Co₄N Matrix as an efficient electrocatalyst for hydrogen generation. *ACS Nano* 2022;16:18038-47. DOI
 41. Yang Y, Yang Q, Yang Y, et al. Enhancing water oxidation of Ru single atoms via oxygen-coordination bonding with NiFe layered double hydroxide. *ACS Catal* 2023;13:2771-9. DOI
 42. Chen J, Huang B, Cao R, et al. Steering local electronic configuration of Fe-N-C-based coupling catalysts via ligand engineering for efficient oxygen electroreduction. *Adv Funct Mater* 2023;33:2209315. DOI
 43. Ou H, Li G, Ren W, et al. Atomically dispersed Au-assisted C-C coupling on red phosphorus for CO₂ photoreduction to C₂H₆. *J Am Chem Soc* 2022;144:22075-82. DOI
 44. Liu F, Xia Y, Xu W, et al. Integration of bimetallic electronic synergy with oxide site isolation improves the selective hydrogenation of acetylene. *Angew Chem Int Ed* 2021;60:19324-30. DOI
 45. Guo Y, Yuan P, Zhang J, et al. Co₂P-CoN double active centers confined in N-doped carbon nanotube: heterostructural engineering for trifunctional catalysis toward HER, ORR, OER, and Zn-air batteries driven water splitting. *Adv Funct Mater* 2018;28:1805641. DOI
 46. Sun Q, Chen BWJ, Wang N, et al. Zeolite-encaged Pd-Mn nanocatalysts for CO₂ hydrogenation and formic acid dehydrogenation. *Angew Chem Int Ed* 2020;59:20183-91. DOI
 47. Liang D, Wang Y, Chen M, et al. Dry reforming of methane for syngas production over attapulgite-derived MFI zeolite encapsulated bimetallic Ni-Co catalysts. *Appl Catal B Environ* 2023;322:122088. DOI
 48. Fang JY, Zheng QZ, Lou YY, et al. Ampere-level current density ammonia electrochemical synthesis using CuCo nanosheets simulating nitrite reductase bifunctional nature. *Nat Commun* 2022;13:7899. DOI PubMed PMC
 49. Aitbekova A, Zhou C, Stone ML, et al. Templated encapsulation of platinum-based catalysts promotes high-temperature stability to 1,100 °C. *Nat Mater* 2022;21:1290-7. DOI
 50. Chi X, Li M, Di J, et al. A highly stable and flexible zeolite electrolyte solid-state Li-air battery. *Nature* 2021;592:551-7. DOI
 51. Zhao H, Yu R, Ma S, et al. The role of CuI-O₃ species in single-atom Cu/ZrO₂ catalyst for CO₂ hydrogenation. *Nat Catal* 2022;5:818-31. DOI
 52. Yuan C, Zeng P, Cheng C, et al. Boosting the rate performance of Li-S batteries via highly dispersed cobalt nanoparticles embedded into nitrogen-doped hierarchical porous carbon. *CCS Chem* 2022;4:2829-41. DOI
 53. Zhao Y, Pei Z, Lu XF, Luan D, Wang X, Lou XW. Rationally designed nitrogen-doped carbon macroporous fibers with loading of single cobalt sites for efficient aqueous Zn-CO₂ batteries. *Chem Catal* 2022;2:1480-93. DOI
 54. Su Y, Hao J, Liu X, Yang Y. Progress of atomic layer deposition and molecular layer deposition in the development of all-solid-state lithium batteries. *Batteries Supercaps* 2023;6:e202200359. DOI
 55. Wen Z, Zhang S, Liu Z, et al. Size-engineered noble metal nanoclusters synthesized by impregnation for size-dependent catalysis. *Sci China Mater* 2023;66:1417-26. DOI
 56. Jiang L, Luo X, Wang D. A review on system and materials for aqueous flexible metal-air batteries. *Carbon Energy* 2023;5:e284. DOI
 57. Zhao Y, Shi Z, Zhu Y, et al. Mechanism for one-pot synthesis of 0D-2D carbon materials in the bubbles inside molten salts. *Adv Funct Mater* 2022;32:2202381. DOI
 58. Hou S, Zhang A, Zhou Q, et al. Designing heterostructured FeP-CoP for oxygen evolution reaction: interface engineering to enhance electrocatalytic performance. *Nano Res* 2023;16:6601-7. DOI
 59. Xia H, Zan L, Qu G, et al. Evolution of a solid electrolyte interphase enabled by FeN_x/C catalysts for sodium-ion storage. *Energy Environ Sci* 2022;15:771-9. DOI
 60. Xia H, Yuan P, Zan L, et al. Probing the active sites of 2D nanosheets with Fe-N-C carbon shell encapsulated Fe₃C/Fe species for boosting sodium-ion storage performances. *Nano Res* 2022;15:7154-62. DOI
 61. Zhao B, Huang X, Ding Y, Bi Y. Bias-free solar-driven syngas production: a Fe₂O₃ photoanode featuring single-atom cobalt integrated with a silver-palladium cathode. *Angew Chem Int Ed* 2023;62:e202213067. DOI
 62. Ma Z, Liu S, Tang N, et al. Coexistence of Fe nanoclusters boosting Fe single atoms to generate singlet oxygen for efficient aerobic oxidation of primary amines to imines. *ACS Catal* 2022;12:5595-604. DOI
 63. Xue D, Cheng J, Yuan P, et al. Boron-tethering and regulative electronic states around iridium species for hydrogen evolution. *Adv Funct Mater* 2022;32:2113191. DOI
 64. Yin Z, Yu J, Xie Z, et al. Hybrid catalyst coupling single-atom Ni and nanoscale Cu for efficient CO₂ electroreduction to ethylene. *J Am Chem Soc* 2022;144:20931-8. DOI

65. Xiao F, Wang Y, Xu GL, et al. Fe-N-C boosts the stability of supported platinum nanoparticles for fuel cells. *J Am Chem Soc* 2022;144:20372-84. DOI
66. Zhang X, Zhang M, Deng Y, et al. A stable low-temperature H₂-production catalyst by crowding Pt on α -MoC. *Nature* 2021;589:396-401. DOI
67. Qiao B, Wang A, Yang X, et al. Single-atom catalysis of CO oxidation using Pt₁/FeO_x. *Nat Chem* 2011;3:634-41. DOI
68. Sun L, Reddu V, Wang X. Multi-atom cluster catalysts for efficient electrocatalysis. *Chem Soc Rev* 2022;51:8923-56. DOI PubMed
69. Zhao YX, Wen JH, Li P, et al. A “pre-division metal clusters” strategy to mediate efficient dual-active sites ORR catalyst for ultralong rechargeable Zn-air battery. *Angew Chem Int Ed* 2023;62:e202216950. DOI
70. Han J, Liu R, Lin Z, Zi W. Stereodivergent construction of Csp³-Csp³ bonds bearing vicinal stereocenters by synergistic palladium and phase-transfer catalysis. *Angew Chem Int Ed* 2023;62:e202215714. DOI
71. Ye Y, Cao J, Oblinsky DG, et al. Using enzymes to tame nitrogen-centred radicals for enantioselective hydroamination. *Nat Chem* 2023;15:206-12. DOI
72. Shi J. On the synergetic catalytic effect in heterogeneous nanocomposite catalysts. *Chem Rev* 2013;113:2139-81. DOI PubMed
73. Liu H, Lang X, Zhu C, et al. Efficient electrochemical nitrate reduction to ammonia with copper-supported rhodium cluster and single-atom catalysts. *Angew Chem Int Ed* 2022;61:e202202556. DOI
74. Ding S, He L, Fang L, et al. Carbon-nanotube-bridging strategy for integrating single Fe atoms and NiCo nanoparticles in a bifunctional oxygen electrocatalyst toward high-efficiency and long-life rechargeable zinc-air batteries. *Adv Energy Mater* 2022;12:2202984. DOI
75. Guo W, Gao X, Zhu M, et al. A closely packed Pt_{1.5}Ni_{1.5}/Ni-N-C hybrid for relay catalysis towards oxygen reduction. *Energy Environ Sci* 2023;16:148-56. DOI
76. Zhang L, Jang H, Wang Y, et al. Exploring the dominant role of atomic- and nano-ruthenium as active sites for hydrogen evolution reaction in both acidic and alkaline media. *Adv Sci* 2021;8:e2004516. DOI PubMed PMC
77. Su P, Pei W, Wang X, et al. Exceptional electrochemical HER performance with enhanced electron transfer between Ru nanoparticles and single atoms dispersed on a carbon substrate. *Angew Chem Int Ed* 2021;60:16044-50. DOI
78. Yang X, Wang Y, Wang X, et al. CO-tolerant PEMFC anodes enabled by synergistic catalysis between iridium single-atom sites and nanoparticles. *Angew Chem Int Ed* 2021;60:26177-83. DOI
79. Guo S, Su J, Luo H, et al. Boosting photocatalytic hydrogen evolution reaction by the improved mass flow and energy flow process based on ultrasound waves. *ACS Catal* 2023;13:296-307. DOI
80. Wei P, Chen Y, Zhou T, et al. Manipulation of charge-transfer kinetics via Ti₃C₂T_x (T = -O) quantum dot and N-doped carbon dot coloaded on CdS for photocatalytic hydrogen production. *ACS Catal* 2023;13:587-600. DOI
81. Zhu J, Cao J, Cai G, et al. Non-trivial contribution of carbon hybridization in carbon-based substrates to electrocatalytic activities in Li-S batteries. *Angew Chem Int Ed* 2023;62:e202214351. DOI
82. Wei H, Liu H, Yu L, et al. Alloying Pd with Cu boosts hydrogen production via room-temperature electrochemical water-gas shift reaction. *Nano Energy* 2022;102:107704. DOI
83. Zhang L, Ren X, Zhao X, et al. Synergetic charge transfer and spin selection in CO oxidation at neighboring magnetic single-atom catalyst sites. *Nano Lett* 2022;22:3744-50. DOI
84. Huang H, Yu D, Hu F, et al. Clusters induced electron redistribution to tune oxygen reduction activity of transition metal single-atom for metal-air batteries. *Angew Chem Int Ed* 2022;61:e202116068. DOI
85. Chen M, Kong F, Yao H, et al. Dual metal-organic frameworks-derived Fe-atomic sites bounded to fine Fe/Fe_xC nanoparticles for enhanced oxygen electroreduction. *Chem Eng J* 2023;453:139820. DOI
86. Yao H, Wang X, Li K, et al. Strong electronic coupling between ruthenium single atoms and ultrafine nanoclusters enables economical and effective hydrogen production. *Appl Catal B Environ* 2022;312:121378. DOI
87. Bae S, Mahmood J, Jeon I, Baek J. Recent advances in ruthenium-based electrocatalysts for the hydrogen evolution reaction. *Nanoscale Horiz* 2020;5:43-56. DOI
88. Hu Q, Li G, Huang X, et al. Electronic structure engineering of single atomic Ru by Ru nanoparticles to enable enhanced activity for alkaline water reduction. *J Mater Chem A* 2019;7:19531-8. DOI
89. Yu Y, Xue D, Xia H, et al. Electron spin modulation engineering in oxygen-involved electrocatalysis. *J Phys Condens Matter* 2022;34:364002. DOI
90. Tian Y, Cao H, Yang H, et al. Electron spin catalysis with graphene belts. *Angew Chem Int Ed* 2023;62:e202215295. DOI
91. Chen W, Xia H, Guo K, et al. Atomically dispersed Fe-N₄ sites and Fe₃C particles catalyzing polysulfides conversion in Li-S batteries. *Chem Res Chin Univ* 2022;38:1232-8. DOI
92. Qu G, Guo K, Dong J, et al. Tuning Fe-spin state of FeN₄ structure by axial bonds as efficient catalyst in Li-S batteries. *Energy Stor Mater* 2023;55:490-7. DOI
93. Yang G, Zhu J, Yuan P, et al. Regulating Fe-spin state by atomically dispersed Mn-N in Fe-N-C catalysts with high oxygen reduction activity. *Nat Commun* 2021;12:1734. DOI PubMed PMC
94. Wei X, Song S, Cai W, et al. Tuning the spin state of Fe single atoms by Pd nanoclusters enables robust oxygen reduction with dissociative pathway. *Chem* 2023;9:181-97. DOI
95. Liu Y, Liu X, Lv Z, et al. Tuning the spin state of the iron center by bridge-bonded Fe-O-Ti ligands for enhanced oxygen reduction. *Angew Chem Int Ed* 2022;61:e202117617. DOI

96. Yang J, Li WH, Tan S, et al. The electronic metal-support interaction directing the design of single atomic site catalysts: achieving high efficiency towards hydrogen evolution. *Angew Chem Int Ed* 2021;60:19085-91. [DOI](#)
97. Yang J, Li W, Wang D, Li Y. Electronic metal-support interaction of single-atom catalysts and applications in electrocatalysis. *Adv Mater* 2020;32:e2003300. [DOI](#)
98. Hu P, Huang Z, Amghouz Z, et al. Electronic metal-support interactions in single-atom catalysts. *Angew Chem Int Ed* 2014;53:3418-21. [DOI](#)
99. Liu P, Chen B, Liang C, et al. Tip-enhanced electric field: a new mechanism promoting mass transfer in oxygen evolution reactions. *Adv Mater* 2021;33:e2007377. [DOI](#)
100. Khan MU, Wang L, Liu Z, et al. Pt₃Co octapods as superior catalysts of CO₂ hydrogenation. *Angew Chem Int Ed* 2016;55:9548-52. [DOI](#)
101. Yu J, Yin J, Li R, Ma Y, Fan Z. Interfacial electric field effect on electrochemical carbon dioxide reduction reaction. *Chem Catal* 2022;2:2229-52. [DOI](#)
102. Liu W, Li X, Wang Y, et al. Multi-branched AgAuPt nanoparticles for efficient electrocatalytic hydrogen evolution: synergism of tip-enhanced electric field effect and local electric field effect. *J Energy Chem* 2023;81:339-48. [DOI](#)
103. Wang L, Wang L, Zhang L, Liu H, Yang J. Perspective of *p*-block single-atom catalysts for electrocatalysis. *Trends Chem* 2022;4:1135-48. [DOI](#)
104. Yan H, Xiang H, Liu J, et al. The factors dictating properties of atomically precise metal nanocluster electrocatalysts. *Small* 2022;18:e2200812. [DOI](#)
105. Yang J, Li WH, Xu K, Tan S, Wang D, Li Y. Regulating the tip effect on single-atom and cluster catalysts: forming reversible oxygen species with high efficiency in chlorine evolution reaction. *Angew Chem Int Ed* 2022;61:e202200366. [DOI](#)
106. Zhou W, Jiang Z, Chen M, et al. Directly anchoring non-noble metal single atoms on 1T-TMDs with tip structure for efficient hydrogen evolution. *Chem Eng J* 2022;428:131210. [DOI](#)
107. Xia H, Zan L, Yuan P, et al. Evolution of stabilized 1T-MoS₂ by atomic-interface engineering of 2H-MoS₂/Fe-N_x towards enhanced sodium ion storage. *Angew Chem Int Ed* 2023;62:e202218282. [DOI](#)
108. Ma Q, Jin H, Zhu J, et al. Stabilizing Fe-N-C catalysts as model for oxygen reduction reaction. *Adv Sci* 2021;8:e2102209. [DOI](#) [PubMed](#) [PMC](#)
109. Chipman J. Thermodynamics and phase diagram of the Fe-C system. *Metall Trans* 1972;3:55-64. [DOI](#)
110. Ao X, Zhang W, Li Z, et al. Markedly enhanced oxygen reduction activity of single-atom Fe catalysts via integration with Fe nanoclusters. *ACS Nano* 2019;13:11853-62. [DOI](#)
111. Wan X, Liu Q, Liu J, et al. Iron atom-cluster interactions increase activity and improve durability in Fe-N-C fuel cells. *Nat Commun* 2022;13:2963. [DOI](#) [PubMed](#) [PMC](#)
112. Xie S, Liu L, Lu Y, et al. Pt atomic single-layer catalyst embedded in defect-enriched ceria for efficient CO oxidation. *J Am Chem Soc* 2022;144:21255-66. [DOI](#)
113. Chen L, Zhang X, Chen A, Yao S, Hu X, Zhou Z. Targeted design of advanced electrocatalysts by machine learning. *Chin J Catal* 2022;43:11-32. [DOI](#)
114. Hu X, Chen S, Chen L, et al. What is the real origin of the activity of Fe-N-C electrocatalysts in the O₂ reduction reaction? Critical roles of coordinating pyrrolic N and axially adsorbing species. *J Am Chem Soc* 2022;144:18144-52. [DOI](#)